European Journal of Medicinal Chemistry 263 (2024) 115916

Contents lists available at ScienceDirect

European Journal of Medicinal Chemistry

journal homepage: www.elsevier.com/locate/ejmech

Research paper

Design, synthesis, ADME and biological evaluation of benzylpiperidine and benzylpiperazine derivatives as novel reversible monoacylglycerol lipase (MAGL) inhibitors

Miriana Di Stefano [a,b,1], Samuele Masoni [a,1], Giulia Bononi [a], Giulio Poli [a], Salvatore Galati [a], Francesca Gado [c], Simone Manzi [c], Chiara Vagaggini [d], Annalaura Brai [d], Isabella Caligiuri [e], Kanwal Asif [f], Flavio Rizzolio [e,f], Marco Macchia [a], Andrea Chicca [g], Andrea Sodi [i], Valeria Di Bussolo [a], Filippo Minutolo [a,h], Philip Meier [g], Jürg Gertsch [g], Carlotta Granchi [a,h,*], Elena Dreassi [d], Tiziano Tuccinardi [a,h]

[a] Department of Pharmacy, University of Pisa, Via Bonanno 6, 56126, Pisa, Italy
[b] Department of Life Sciences, University of Siena, Via Aldo Moro, 2, 53100, Siena, Italy
[c] Department of Pharmaceutical Sciences, University of Milan, Via Luigi Mangiagalli 25, 20133, Milan, Italy
[d] Department of Biotechnology, Chemistry and Pharmacy, University of Siena, Via Aldo Moro, 2, 53100, Siena, Italy
[e] Pathology Unit, Centro di Riferimento Oncologico di Aviano (CRO) IRCCS, 33081, Aviano, Italy
[f] Department of Molecular Sciences and Nanosystems, Ca' Foscari University, 30123, Venezia, Italy
[g] Institute of Biochemistry and Molecular Medicine, NCCR TransCure, University of Bern, CH-3012, Bern, Switzerland
[h] Center for Instrument Sharing of the University of Pisa (CISUP), Lungarno Pacinotti 43, 56126, Pisa, Italy
[i] Department of Neurosciences, Psychology, Drug Research and Child Health Eye Clinic, University of Florence, AOU Careggi, 50139, Florence, Italy

ARTICLE INFO

Keywords:
Monoacylglycerol lipase
MAGL
Inhibitors
Benzylpiperidine
Benzylpiperazine
ADME

ABSTRACT

The degradation of the endocannabinoid 2-arachidonoylglycerol is mediated by the enzyme monoacylglycerol lipase (MAGL), thus generating arachidonic acid, the precursor of prostaglandins and other pro-inflammatory mediators. MAGL also contributes to the hydrolysis of monoacylglycerols into glycerol and fatty acids in peripheral body districts, which may act as pro-tumorigenic signals. For this reason, MAGL inhibitors have been considered as interesting therapeutic agents for their anti-nociceptive, anti-inflammatory, antioxidant and anticancer properties. So far, only a limited series of reversible MAGL inhibitors, which are devoid of side effects shown by irreversible inhibitors in animal models, have been reported. Here we optimized a class of benzylpiperidine and benzylpiperazine-based compounds for a reversible MAGL inhibition. The best MAGL inhibitors of this class, compounds **28** and **29**, showed a very good inhibition potency, both on the isolated enzyme and in U937 cells, as confirmed by molecular modeling studies that predicted their binding mode into the MAGL active site. Both compounds are characterized by a high selectivity for MAGL *versus* other serine hydrolases including enzymes of the endocannabinoid system, as confirmed by ABPP experiments in mouse brain membranes. Moreover, very good properties concerning ADME parameters and low *in vivo* toxicity have been observed for both compounds.

1. Introduction

The endocannabinoid system (ECS) is primarily composed by a set of endogenous lipid derivatives (endocannabinoids), their G-protein coupled receptors and proteins for biosynthesis and degradation of endocannabinoids. The two major endocannabinoids, 2-arachidonoylglycerol (2-AG) and *N*-arachidonoylethanolamide (AEA or anandamide) are endogenous ligands of cannabinoid receptors (CBRs) CB1 and CB2 and play important roles in a wide range of physiological and pathological processes both in the central nervous system and in peripheral organs [1]. Unlike classical neurotransmitters,

* Corresponding author. Department of Pharmacy, University of Pisa, Italy.
E-mail address: carlotta.granchi@unipi.it (C. Granchi).
[1] These authors equally contributed to this work.

https://doi.org/10.1016/j.ejmech.2023.115916
Received 1 August 2023; Received in revised form 17 October 2023; Accepted 25 October 2023
Available online 2 November 2023
0223-5234/© 2023 The Authors. Published by Elsevier Masson SAS. This is an open access article under the CC BY license (http://creativecommons.org/licenses/by/4.0/).

Abbreviations

2-AG	2-arachidonoylglycerol
2-OG	2-oleoylglycerol
4-NPA	4-nitrophenylacetate
9-BBN	9-borabicyclo[3.3.1]nonane
AA	arachidonic acid
ABHD6	α/β hydrolase-6
ABHD12	α/β hydrolase-12
ABPP	activity-based protein profiling
AEA	anandamide
BSA	bovine serum albumin
CBR	cannabinoid receptor
CG	conjugate gradient
DIPEA	*N,N*-diisopropylethylamine
DMF	*N,N*-dimethylformamide
DTT	1,4-dithio-dl-threitol
ECS	endocannabinoid system
MEMFAAH	fatty acid amide hydrolase
GAFF	General Amber force field
HATU	1-[bis(dimethylamino)methylene]-1*H*-1,2,3-triazolo[4,5-*b*]pyridinium 3-oxide hexafluorophosphate
MAGL	monoacylglycerol lipase
MD	molecular dynamics
MEM	methoxyethoxymethyl
PAMPA	Parallel Artificial Membrane Permeability Assay
PME	Particle Mesh Ewald
TLC	thin layer chromatography
TMC	*Tenebrio molitor* coleoptera

endocannabinoids are produced on demand and are rapidly inactivated, after the activation of their targets, by cellular uptake and enzymatic hydrolysis. AEA is metabolized into arachidonic acid (AA) and ethanolamine by fatty acid amide hydrolase (FAAH), and 2-AG is mainly hydrolyzed and inactivated by monoacylglycerol lipase (MAGL), a 33-kDa membrane-associated serine hydrolase containing a Ser122/-His269/Asp239 catalytic triad. Despite MAGL is the main contributor to 2-AG degradation by metabolizing about 85 % of 2-AG into AA and glycerol, enzymes α/β-hydrolase domain containing 6 and α/β-hydrolase domain containing 12 (ABHD6 and ABDH12) hydrolyze the remaining 15 % [2,3]. The significant immune-modulatory, neuroprotective and anti-inflammatory properties exerted by 2-AG are widely documented and reviewed in literature [4,5]. Unfortunately, the direct activation of CB1 is also responsible for unwanted psychoactive side effects, such as dizziness, euphoria and addiction. Among different strategies, an alternative approach to target CB1 and CB2 is represented by MAGL inhibition, which leads to consequent enhancement of 2-AG signaling, resulting in an indirect CBRs activation, thus preserving the beneficial effects derived from direct activation, but limiting potential side effects mostly associated to direct CB1 activation [6]. Moreover, MAGL is highly expressed in aggressive cancers and primary tumors, controlling free fatty acid levels, which are precursors for pro-tumorigenic signaling lipids, thus MAGL inhibition determines a reduction of cancer cell growth and invasiveness in some aggressive cancer types [7,8]. For these reasons, MAGL has received great attention as a promising therapeutic target against a plethora of pathological conditions including cancer, neurological disorders such as multiple sclerosis, amyotrophic lateral sclerosis, Alzheimer's diseases and Parkinson's diseases, and inflammatory pathologies [9]. Several academic groups and pharmaceutical companies have developed MAGL inhibitors having a reversible or irreversible mode of action. Despite the high inhibition potency shown by most of the irreversible MAGL inhibitors, the

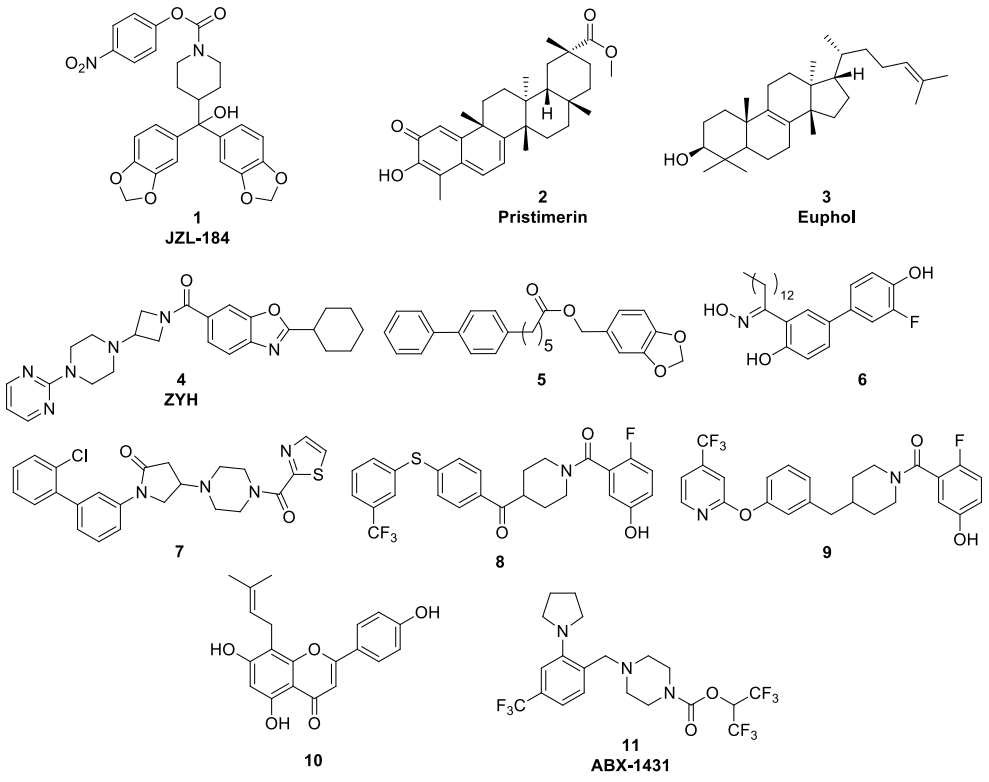

Fig. 1. Structures of some representative MAGL inhibitors.

main limit of these compounds is their side effects when tested *in vivo*, since prolonged high levels of 2-AG lead to CB1 desensitization. Moreover, mice treated with irreversible MAGL inhibitors and MAGL-deficient mice showed impaired CB1-dependent synaptic plasticity, cross-tolerance to exogenous CB1 agonists and physical dependence [10–14]. Most of these effects were observed after administration of compound **1** (JZL-184, 4-nitrophenyl-4-[bis(1,3-benzodioxol-5-yl)(hydroxy)methyl]piperidine-1-carboxylate, Fig. 1), a very potent carbamate-based irreversible inhibitor [15], which at present represents a milestone among MAGL inhibitors, but its further development was limited due to its considerable side effects. Among the most representative natural MAGL inhibitors were the two triterpenes Pristimerin **2** (Fig. 1) and Euphol **3** (Fig. 1), which were the first two compounds identified as MAGL inhibitors in 2009. However, their low selectivity limited their further development [16,17]. In the group of synthetic MAGL inhibitors, it is noteworthy to cite (2-cyclohexyl-1,3-benzoxazol-6-yl){3-[4-(pyrimidin-2-yl)piperazin-1-yl]azetidin-1-yl}methanone ZYH **4** (Fig. 1) which was co-crystallized with human MAGL and the high-resolution X-ray structure revealed the conformational changes of the protein during the catalytic cycle [18], thus giving useful insights for the development of MAGL ligands. Some years later, reversible MAGL inhibitor benzo [*d*] [1,3]dioxol-5-ylmethyl 6-phenylhexanoate **5** (Fig. 1) was tested in an experimental autoimmune encephalomyelitis multiple sclerosis mouse model, in which it improved the clinical progression of the disease without provoking undesirable CB1-mediated side effects [19]. A salicylketoxime-based MAGL inhibitor **6** (Fig. 1) demonstrated further potential therapeutic applications of MAGL blockade, by showing promising antiproliferative activities in a series of cancer cell lines [20]. Takeda Pharmaceuticals developed the piperazinyl pyrrolidin-2-one **7** (Fig. 1) which proved to be a potent MAGL inhibitor both *in vitro* and *in vivo*, since it increased 2-AG level, thus reducing AA concentration in mouse brains [21]. Compounds **8** [22] and **9** [23] (Fig. 1) are the most recent examples belonging to the chemical classes of benzoylpiperidine and benzylpiperidine-based MAGL inhibitors, respectively, developed by our research group in the last years: these compounds reached nanomolar inhibition values on the isolated enzyme and showed antiproliferative activities in cancer cells. Recently, natural compound **10** (Fig. 1) was isolated from the plant *Humulus lupulus* L. and showed an acceptable inhibition activity on human MAGL [24]. Carbamate-based MAGL inhibitor **11** (ABX-1431, Fig. 1) was

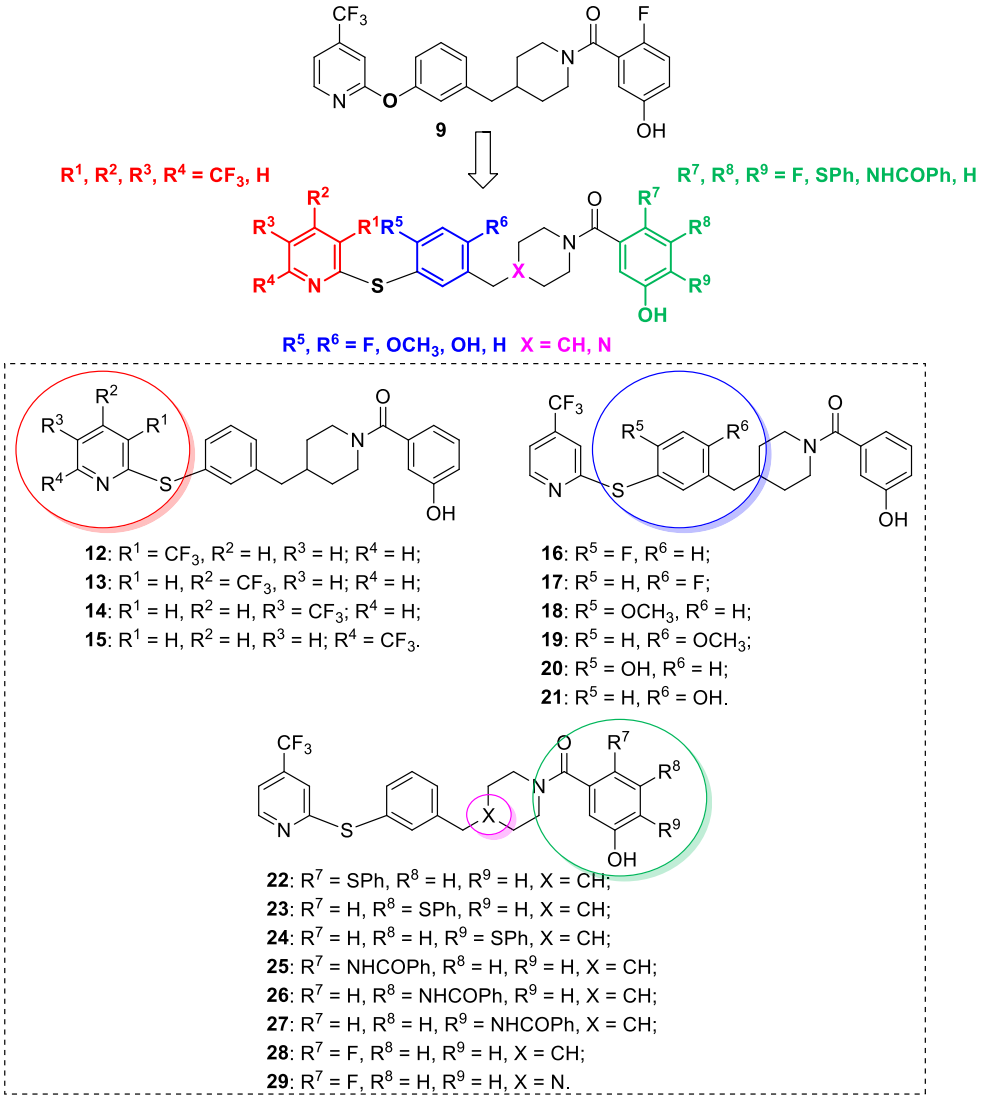

Fig. 2. Design of new derivatives **12**–**29**. Benzylpiperidine **9** is the parent compound and the newly synthesized derivatives **12**–**29** are reported below (dashed square). Substitutions on the pyridine ring (compounds **12**–**15**) are highlighted in red, substitutions on the phenyl ring (compounds **16**–**21**) are highlighted in blue and substitutions on the phenolic ring (compounds **22**–**28**) are highlighted in green. Replacement of the piperidine with a piperazine ring is highlighted in magenta (compound **29**).

identified by Cisar et al. at Abide Therapeutics [25] as a promising clinical candidate for patients suffering of neurological disorders. Interestingly, this compound was evaluated in clinical trials for the treatment of central neuropathic pain, in particular in neuromyelitis optica spectrum disorder, transverse myelitis, longitudinally extensive transverse myelitis and multiple sclerosis.

2. Results and discussion

2.1. Design of new benzylpiperidine derivatives

The discovery of benzylpiperidine MAGL inhibitor **9** previously made by our research group [23] prompted us to further explore this chemical scaffold as an effective source of new potential MAGL inhibitors. The first step was the replacement of the oxygen atom as the linker between the pyridine and the central phenyl ring with a sulphur atom, considering that sulphur is a classic isostere for oxygen. Moreover, we decided to further investigate the influence of substituents on the pyridine and the central phenyl ring with a series of exploratory simple substitution patterns (trifluoromethyl, fluorine, methoxy and hydroxyl group), which were selected to determine if their presence could be beneficial for MAGL inhibition, also taking into consideration the easy commercial availability of the corresponding chemical precursors. This strategy gave rise to compounds **12**–**15** which are substituted on the pyridine ring (R^1, R^2, R^3 and R^4 in red, Fig. 2) and compounds **16**–**21** which are substituted on the central phenyl ring (R^5 and R^6 in blue, Fig. 2). Another modification was focused on the phenolic ring, considering the binding mode of the parent compound **9** into the MAGL active site: molecular modeling studies demonstrated that its disposition is shifted toward the entrance of the binding site compared to the previously developed benzoylpiperidine-based MAGL inhibitors (here exemplified by compound **8**, Fig. 1) [22], however compound **9** still maintains some key H-bond interactions in the MAGL binding site [23]. This binding mode allowed us to insert some substituents on the phenolic ring, ranging from small groups, such as a fluorine atom in *para* position to the hydroxyl group, which was highly beneficial for MAGL inhibition potency in the previous series of benzylpiperidine derivatives [23], to bulkier moieties such as a phenyl ring linked to the phenolic portion by means of a simple sulphur atom or an amide group, thus obtaining compounds **22**–**28** (R^7, R^8 and R^9 in green, Fig. 2). Finally, we were intrigued by the possibility of replacing the piperidine with a piperazine ring, hence we planned to synthesize benzylpiperazine derivative **29** (Fig. 2), with the aim of assessing the influence of an aliphatic tertiary amino group on MAGL activity.

2.2. Chemistry

The synthesis started with the preparation of amine hydrochlorides **55**–**62**: in the first step commercially available trifluoromethyl-substituted 2-chloropyridines **30**–**33** reacted with 3-bromothiophenol **34**, fluoro-substituted bromothiophenols **35** and **36** or methoxy-substituted bromothiophenols **37** and **38** in the presence of potassium carbonate as the base and *N*,*N*-dimethylformamide (DMF) as the solvent (Scheme 1) to give diarylsulfide derivatives **39**–**46**. A hydroboration procedure with 9-borabicyclo [3.3.1]nonane (9-BBN) of alkene moiety of 1-Boc-4-methylenepiperidine followed by a cross coupling reaction catalyzed by tetrakis (triphenylphosphine)palladium (0) with brominated intermediates **39**–**46**, as previously reported [23], allowed to build the benzylpiperidine scaffold of compounds **47**–**54** (Scheme 1), which were finally deprotected by using HCl in dioxane to obtain piperidine hydrochlorides **55**–**62** (Scheme 1).

At the same time, properly substituted benzoic acids **68a-c**, **70a,b** and **72** were prepared starting from esterification of amino or bromo-substituted 3-methoxybenzoic acids (Scheme 2). In the case of amino-substituted 3-methoxybenzoic acids **64a,b**, they were converted to the corresponding methyl esters **66a,b** by refluxing them with thionyl chloride in methanol, whereas bromo-substituted benzoic acids **63a-c** were subjected to Fisher esterification thus obtaining methyl esters **65a-c** (Scheme 2). Intermediates **65a-c** were reacted in a cross-coupling reaction with thiophenol, catalyzed by tris(dibenzylideneacetone)dipalladium with Xantphos as the ligand, to obtain diarylsulfide derivatives **67a-c**, then saponification with lithium hydroxide afforded the desired

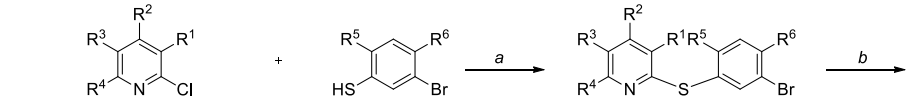

30-33 **34-38** **39-46**

30: $R^1 = CF_3$, $R^2 = H$, $R^3 = H$, $R^4 = H$;
31: $R^1 = H$, $R^2 = CF_3$, $R^3 = H$, $R^4 = H$;
32: $R^1 = H$, $R^2 = H$, $R^3 = CF_3$, $R^4 = H$;
33: $R^1 = H$, $R^2 = H$, $R^3 = H$, $R^4 = CF_3$.

34: $R^5 = H$, $R^6 = H$;
35: $R^5 = F$, $R^6 = H$;
36: $R^5 = H$, $R^6 = F$;
37: $R^5 = OCH_3$, $R^6 = H$;
38: $R^5 = H$, $R^6 = OCH_3$.

39: $R^1 = CF_3$, $R^2 = H$, $R^3 = H$, $R^4 = H$, $R^5 = H$, $R^6 = H$;
40: $R^1 = H$, $R^2 = CF_3$, $R^3 = H$, $R^4 = H$, $R^5 = H$, $R^6 = H$;
41: $R^1 = H$, $R^2 = H$, $R^3 = CF_3$, $R^4 = H$, $R^5 = H$, $R^6 = H$;
42: $R^1 = H$, $R^2 = H$, $R^3 = H$, $R^4 = CF_3$, $R^5 = H$, $R^6 = H$;
43: $R^1 = H$, $R^2 = CF_3$, $R^3 = H$, $R^4 = H$, $R^5 = F$, $R^6 = H$;
44: $R^1 = H$, $R^2 = CF_3$, $R^3 = H$, $R^4 = H$, $R^5 = H$, $R^6 = F$;
45: $R^1 = H$, $R^2 = CF_3$, $R^3 = H$, $R^4 = H$, $R^5 = OCH_3$, $R^6 = H$;
46: $R^1 = H$, $R^2 = CF_3$, $R^3 = H$, $R^4 = H$, $R^5 = H$, $R^6 = OCH_3$.

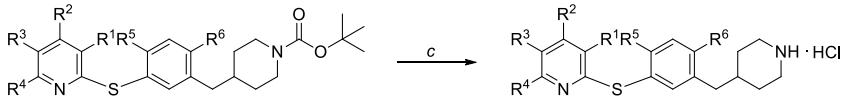

47-54 **55-62**

47: $R^1 = CF_3$, $R^2 = H$, $R^3 = H$, $R^4 = H$, $R^5 = H$, $R^6 = H$;
48: $R^1 = H$, $R^2 = CF_3$, $R^3 = H$, $R^4 = H$, $R^5 = H$, $R^6 = H$;
49: $R^1 = H$, $R^2 = H$, $R^3 = CF_3$, $R^4 = H$, $R^5 = H$, $R^6 = H$;
50: $R^1 = H$, $R^2 = H$, $R^3 = H$, $R^4 = CF_3$, $R^5 = H$, $R^6 = H$;
51: $R^1 = H$, $R^2 = CF_3$, $R^3 = H$, $R^4 = H$, $R^5 = F$, $R^6 = H$;
52: $R^1 = H$, $R^2 = CF_3$, $R^3 = H$, $R^4 = H$, $R^5 = H$, $R^6 = F$;
53: $R^1 = H$, $R^2 = CF_3$, $R^3 = H$, $R^4 = H$, $R^5 = OCH_3$, $R^6 = H$;
54: $R^1 = H$, $R^2 = CF_3$, $R^3 = H$, $R^4 = H$, $R^5 = H$, $R^6 = OCH_3$.

55: $R^1 = CF_3$, $R^2 = H$, $R^3 = H$, $R^4 = H$, $R^5 = H$, $R^6 = H$;
56: $R^1 = H$, $R^2 = CF_3$, $R^3 = H$, $R^4 = H$, $R^5 = H$, $R^6 = H$;
57: $R^1 = H$, $R^2 = H$, $R^3 = CF_3$, $R^4 = H$, $R^5 = H$, $R^6 = H$;
58: $R^1 = H$, $R^2 = H$, $R^3 = H$, $R^4 = CF_3$, $R^5 = H$, $R^6 = H$;
59: $R^1 = H$, $R^2 = CF_3$, $R^3 = H$, $R^4 = H$, $R^5 = F$, $R^6 = H$;
60: $R^1 = H$, $R^2 = CF_3$, $R^3 = H$, $R^4 = H$, $R^5 = H$, $R^6 = F$;
61: $R^1 = H$, $R^2 = CF_3$, $R^3 = H$, $R^4 = H$, $R^5 = OCH_3$, $R^6 = H$;
62: $R^1 = H$, $R^2 = CF_3$, $R^3 = H$, $R^4 = H$, $R^5 = H$, $R^6 = OCH_3$.

Scheme 1. Synthesis of compounds **55**–**62**. *Reagents and conditions:* (*a*) anhydrous K_2CO_3, anhydrous DMF, 110 °C, overnight [62–99 %]; (*b*) i. *tert*-butyl 4-methylenepiperidine-1-carboxylate, 9-BBN 0.5 M solution in THF, anhydrous toluene, 115 °C, 1 h; ii. aq. 3.2 M NaOH, $Pd(PPh_3)_4$, TBAI, anhydrous toluene, 115 °C, 18 h [23–99 %]; (*c*) HCl 4.0 M solution in dioxane, anhydrous MeOH, anhydrous CH_2Cl_2, RT, 1 h [98–99 %].

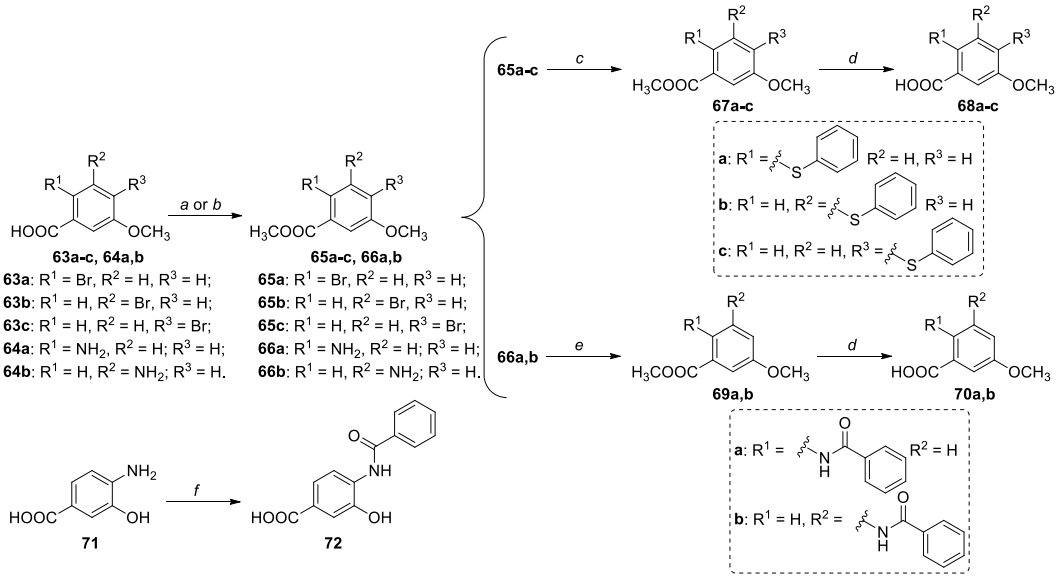

Scheme 2. Synthesis of compounds **68a-c**, **70a,b**, **72**. *Reagents and conditions:* (*a*) for compounds **65a-c**: anhydrous MeOH, conc. H_2SO_4, 80 °C, 2–4 h [81–98 %]; (*b*) for compounds **66a-b**: $SOCl_2$, anhydrous MeOH, 80 °C, 24 h [82–84 %]; (*c*) thiophenol, Pd_2 (dba)$_3$, XantPhos, anhydrous K_2CO_3, anhydrous toluene, 120 °C, 24 h [99 %]; (*d*) aq. 2 N LiOH, THF/MeOH 1:1 *v/v*, RT, overnight [61–99 %]; (*e*) benzoic acid, HATU, DIPEA, anhydrous DMF, RT, 3–12 h [35–83 %]; (*f*) benzoyl chloride, anhydrous pyridine, anhydrous THF, 0 °C, 5 min [99 %].

acids **68a-c** (Scheme 2). Differently, anilines **66a,b** were coupled with benzoic acid in the presence of 1-[bis(dimethylamino)methylene]-1*H*-1,2,3-triazolo [4,5-*b*]pyridinium 3-oxide hexafluorophosphate (HATU) as the condensing agent and *N*,*N*-diisopropylethylamine (DIPEA) as the base, and then methyl ester groups were converted to carboxylic acids thus obtaining compounds **70a,b** (Scheme 2). A different way was followed for 4-amino-3-hydroxybenzoic acid **71**: due to the availability of this hydroxylated precursor in our laboratory instead of the methoxylated counterpart, as in the case of the previously mentioned starting materials, amino group of compound **71** was easily converted to benzamide moiety by using benzoylchloride in pyridine, thus directly affording compound **72** (Scheme 2).

After preparation of suitable amines (Scheme 1) and benzoic acids (Scheme 2), the formation of the corresponding amides was performed as outlined in Scheme 3. Most of the amine precursors (compounds **55**–**62**, Scheme 3) were reacted with properly substituted 3-methoxybenzoic acids **68a-c**, **70a,b** and **73a,b** using the previously reported conditions with HATU and DIPEA. The last step was the deprotection of

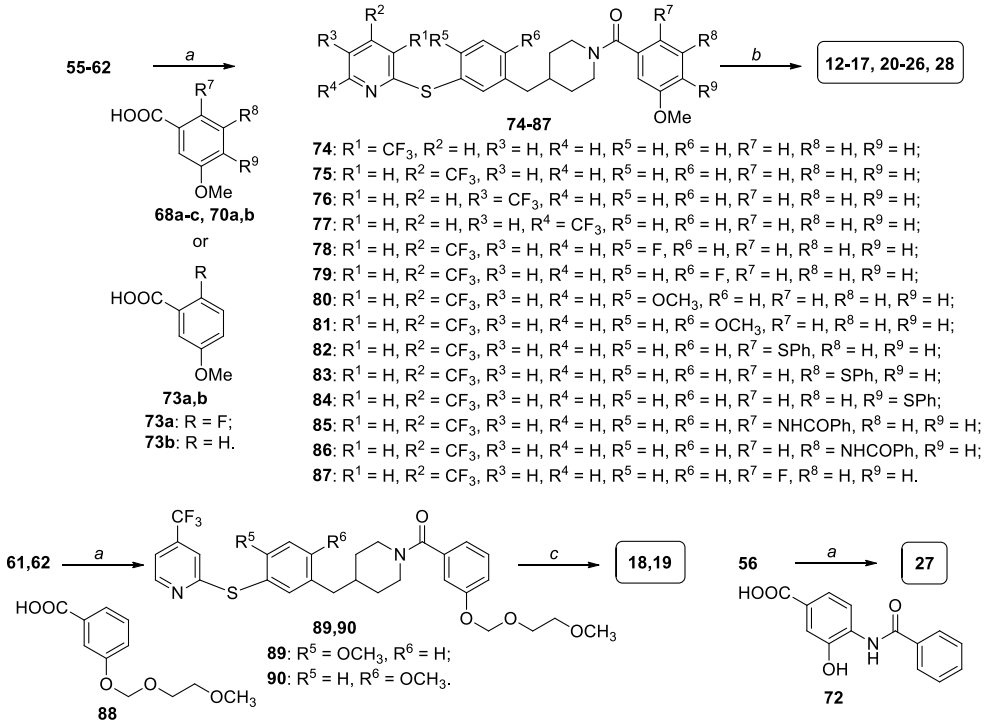

Scheme 3. Synthesis of compounds **12**–**28**. *Reagents and conditions:* (*a*) proper benzoic acid, HATU, DIPEA, anhydrous DMF, RT, 3–12 h [17–66 %]; (*b*) BBr_3, anhydrous CH_2Cl_2, -10 to 0 °C, then RT, 1–2 h [36–75 %]; (*c*) 1 N aq. HCl, CH_3OH, reflux, 2 h [31–78 %].

the methoxy group of intermediates **74**–**87** by boron tribromide in dichloromethane, thus furnishing the final hydroxy-substituted compounds **12**–**17**, **20**–**26** and **28**. A couple of exceptions followed different synthetic strategies: the synthesis of methoxy-substituted derivatives **18** and **19** was accomplished by reacting amines **61,62** with compound **88**, in which the phenolic group was protected with a methoxyethoxymethyl (MEM) ether moiety, which was synthesized as previously reported [22], then MEM protecting group was easily removed by heating reaction crudes **89** and **90** in an acidic methanolic solution (Scheme 3). This different synthetic approach was necessary to maintain the methoxy substituents on the central phenyl ring, thus avoiding their conversion to phenolic groups, which would have been inevitable with the use of boron tribromide as in the case of compounds **74**–**87**. The second exception was the one-step synthesis of compound **27** by using the phenolic derivative **72**, thus avoiding the last deprotection step of the methoxy group, which was instead required for the other compounds (Scheme 3).

Compound **29**, differing from the other final compounds for the presence of a piperazine ring, was synthesized by adopting the synthesis reported in Scheme 4. Fisher esterification of commercially available 3-sulfanylbenzoic acid **91** gave methyl ester **92** (Scheme 4), which was condensed with 2-chloro-4-trifluoromethylpyridine **31**, as reported for intermediates **39**–**46** (Scheme 1), thus obtaining compound **93** (Scheme 4). The methyl ester moiety was reduced to benzyl alcohol by using lithium aluminum hydride and then hydroxyl group was brominated by using phosphorus tribromide to obtain compound **95** (Scheme 4). Reaction with commercially available *tert*-butyl piperazine-1-carboxylate in the presence of sodium hydride, followed by a step aimed at the removal of the *tert*-butyloxycarbonyl protecting group, allowed the formation of piperazine hydrochloride **97** (Scheme 4). Similar to what was described for the other final compounds, the last two steps (steps *g* and *h*, Scheme 4) consisted in amide formation with benzoic acid **73a** and BBr_3-promoted deprotection of the phenolic group, thus finally leading to the formation of desired compound **29**.

2.3. Enzymatic assays

The newly synthesized compounds were tested for their inhibition activities on human MAGL (*h*MAGL) by using a spectrophotometric assay, in which 4-nitrophenylacetate was used as the substrate (Table 1) [26], and the inhibition activities of this series of compounds were compared with the previously published benzylpiperidine MAGL inhibitor **9** [23] and with reference MAGL inhibitor JZL-184 (compound **1**). The first group of compounds (**12**–**15**, Table 1), bearing a trifluoromethyl group in various positions of the pyridine ring, clearly show that the trifluoromethyl group in the *para* position to the pyridine nitrogen atom (R^2, Table 1) gave the best result, as demonstrated by compound **13** showing an IC_{50} value of 2.5 nM (Table 1). The shift of the trifluoromethyl group to other positions of the pyridine ring produced different effects: when the CF_3 group was *ortho* to the sulphur-based linker (R^1 position, Table 1) or *ortho* to the pyridine nitrogen atom (R^4 position, Table 1) the inhibition potencies slightly worsened compared to compound **13**, as for compounds **12** and **15** (IC_{50} values of 7.1 and 13.2 nM, respectively, Table 1), but when the CF_3 was moved to the *para* position to the sulphur-based linker (R^3 position) the activity markedly decreased: indeed, compound **14** displayed an IC_{50} value of 40.4 nM (Table 1). Once the 4-trifluoromethylpyridine portion was assessed as the best substitution pattern, this part of the scaffold was maintained fixed and the subsequent modifications concerned the central phenyl ring (compounds **16**–**21**, Table 1). The presence of a fluorine atom was beneficial for the enzymatic activity when this atom was in the *ortho* position to the sulphur-based linker (R^5 position, Table 1), thus compound **16** showed an excellent IC_{50} value of 2.7 nM. Unfortunately, the fluorine atom in R^6 position did not achieve the same effect and the activity decreased (compound **17**: IC_{50} value of 22.5 nM, Table 1). Similarly, both methoxy and hydroxy groups in the aforementioned positions (R^5 and R^6, compounds **18**–**21**, Table 1) determined a decrease in inhibition potency compared to that of compound **16** (IC_{50} values in the range 14.4–61.2 nM). Among the last group of compounds that are variously substituted in the phenolic ring (**22**–**29**, Table 1), the insertion of a second phenyl ring, which is linked to the phenol by means of a sulphur atom or of an amide moiety was always detrimental for the inhibition potency. It is evident that when the *para* position to the piperidine-amide moiety was occupied the activity had a drastic decrease, as in compounds **24** and **27**, which display IC_{50} values higher than 200 nM. In the case that substituents were in R^7 and R^8 positions, the corresponding inhibition potencies decreased compared to the two best compounds **13** and **16**: the diarylsulfide derivatives **22** and **23** maintained an acceptable level of inhibition with IC_{50} values of 32.3 and 44.8 nM, respectively (Table 1), whereas compounds **25** and **26** showed a more evident loss of activity (IC_{50} values of 112 and 149 nM, respectively, Table 1) likely due to their bulkier substituents. The best result was obtained by introducing a fluorine atom in *para* position to the phenolic group: compound **28** showed the best IC_{50} value of this series of derivatives of 1.3 nM, thus being more potent than the previously published analogue **9**. Lastly, compound **29** differs from **28** only for the piperazine instead of the piperidine ring: this modification had only a slight impact on the enzymatic potency, since **29** maintained a good activity, displaying an IC_{50} value of 5.2 nM (Table 1).

To verify whether this class of compounds could interact with

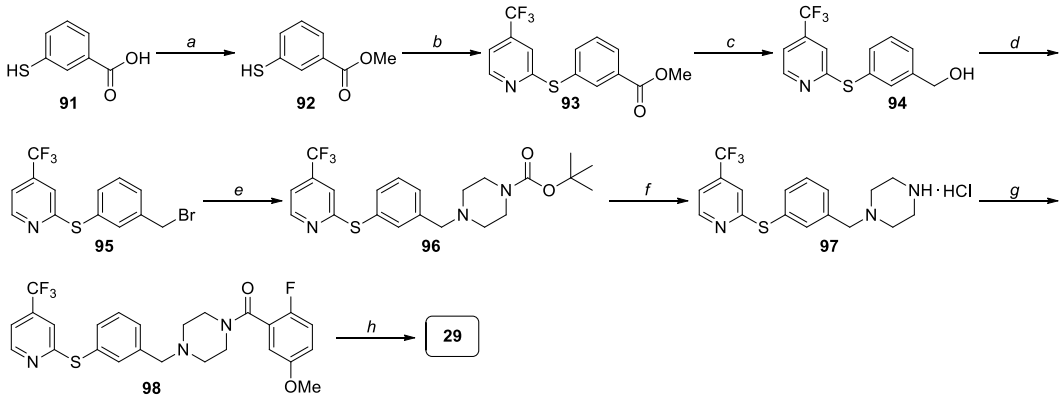

Scheme 4. Synthesis of compound **29**. *Reagents and conditions:* (*a*) anhydrous MeOH, conc. H_2SO_4, 80 °C, 4 h [63 %]; (*b*) **31**, anhydrous K_2CO_3, anhydrous DMF, 110 °C, overnight [60 %]; (*c*) $LiAlH_4$, anhydrous THF, 0 °C, then RT, 1 h [63 %]; (*d*) PBr_3, DCM, 0 °C, then RT, 2 h [40 %]; (*e*) NaH 60 %, *tert*-butyl piperazine-1-carboxylate, anhydrous DMF, 0 °C to RT, 24 h [81 %]; (*f*) HCl 4.0 M solution in dioxane, anhydrous MeOH, anhydrous CH_2Cl_2, RT, 2 h [99 %]; (*g*) **73a**, HATU, DIPEA, anhydrous DMF, RT, 3–12 h [71 %]; (*h*) BBr_3, anhydrous CH_2Cl_2, -10 to 0 °C, then RT, 2 h [60 %].

Table 1
In vitro inhibitory activity on human MAGL (*h*MAGL, IC_{50}, nM)[a] of derivatives **12**–**29**, in comparison with compounds **1** and **9**.

Cpd

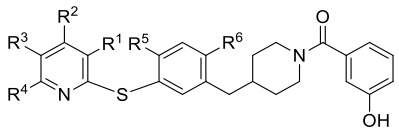

*h*MAGL IC_{50} (nM)

	R^1	R^2	R^3	R^4	R^5	R^6	
12	CF_3	H	H	H	H	H	7.1 ± 0.9
13	H	CF_3	H	H	H	H	2.5 ± 0.4
14	H	H	CF_3	H	H	H	40.4 ± 4.7
15	H	H	H	CF_3	H	H	13.2 ± 2.6
16	H	CF_3	H	H	F	H	2.7 ± 0.1
17	H	CF_3	H	H	H	F	22.5 ± 2.0
18	H	CF_3	H	H	OCH_3	H	14.4 ± 0.9
19	H	CF_3	H	H	H	OCH_3	49.1 ± 2.0
20	H	CF_3	H	H	OH	H	61.2 ± 2.5
21	H	CF_3	H	H	H	OH	20.8 ± 3.2

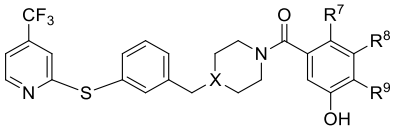

	X	R^7	R^8	R^9	
22	CH	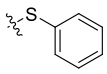	H	H	32.3 ± 0.6
23	CH	H	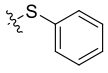	H	44.8 ± 0.1
24	CH	H	H	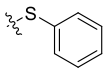	242 ± 20
25	CH	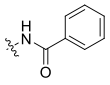	H	H	112 ± 2
26	CH	H	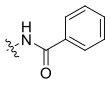	H	149 ± 1
27	CH	H	H	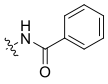	>1000
28	CH	F	H	H	1.3 ± 0.1
29	N	F	H	H	5.2 ± 0.1
1					47 ± 2.1
9					2.1 ± 0.1

[a] Enzymatic values are the mean of three or more independent experiments, performed in duplicates.

cysteine residues of MAGL, the activity of compounds **13**, **16**, **28** and **29** were tested in presence of the thiol-containing agent 1,4-dithio-DL-threitol (DTT). As shown in Fig. 3A, the IC_{50} values of the compounds were not significantly influenced by the presence of DTT, thus excluding any significant interaction with MAGL cysteine residues. Furthermore, to confirm the reversible inhibition mechanism, the four compounds were also subjected to pre-incubation and dilution assays. As shown in Fig. 3B, the pre-incubation test suggests a reversible binding mode for all compounds, as they showed very similar activities at all three different incubation times. As a second test, the effect of dilution on the inhibition activity was investigated. The inhibition produced by incubation with a concentration of 320 nM of compounds **13**, **16**, **28** and **29** was compared with the inhibition produced by a 40X dilution and, as shown in Fig. 3C, the inhibition produced at a concentration of 320 nM was significantly higher compared with that observed at a 40X dilution, which turned out to be similar to the effect produced by an 8 nM concentration of the compounds, thus clearly supporting a reversible mechanism of inhibition.

2.4. Cell-based assays of MAGL inhibition

In order to confirm the MAGL inhibition of the most promising compounds in a more physiological system, derivatives **13**, **16**, **28** and **29** were tested in intact U937 cells as previously described [27]. As shown in Fig. 4, all four compounds showed IC_{50} values in the nanomolar range and, in accordance with enzymatic assays, compound **29** was slightly less potent (IC_{50} = 489 nM) compared to the other tested inhibitors (IC_{50} range of 193–199 nM, for compounds **13**, **16** and **18**).

2.5. Selectivity assays

Compounds **13**, **16**, **28** and **29** were also profiled for their selectivity towards the other components of the ECS. As shown in Table S1, at the concentration of 10 μM none of the compounds significantly bound to CB1R and CB2R or inhibited ABHD6, ABHD12 and FAAH. Then, with the aim to assess the selectivity of the four MAGL inhibitors in a broader context of the serine hydrolase family, we performed competitive activity-based protein profiling (ABPP) experiments using mouse brain membrane preparations. ABPP is a functional proteomics technology that employs chemical probes that react with mechanistically related classes of enzymes [28]. TAMRA-fluorophosphonate (TAMRA-FP) is used as a chemical probe to visualize and identify serine hydrolases, which include the major eCBs degrading enzymes. This probe is designed to irreversibly bind to the active site of serine hydrolases, forming a covalent bond that allows for the detection and identification of these enzymes [29]. One of the key advantages of ABPP over other approaches is its ability to detect changes in the activity of very low-abundance enzymes in highly complex samples. ABPP also allows for the simultaneous assessment of the potency and selectivity of an inhibitor towards the entire family of serine hydrolases in a specific tissue. Mouse brain membranes were pre-incubated with control (DMSO), compounds **13**, **16**, **28** and **29**, and other known inhibitors of serine hydrolases such as MAGL inhibitor JZL-184 **1** [15], URB597 (FAAH inhibitor) [30], WWL70 (ABHD6 inhibitor) [31], THL (ABHD6 and ABHD12 inhibitor) [32] and MAFP (unselective serine hydrolase inhibitor) [33] as controls. The detected TAMRA-FP signal after SDS-PAGE highlighted that the four compounds at the concentration of 10 μM selectively inhibited MAGL (see the two bands associated with MAGL [34] in Fig. 5), without affecting other serine hydrolases such as FAAH, ABHD6 and ABHD12. Since TAMRA-FP is a highly potent covalent irreversible probe, in this ABPP assay reversible inhibitors (such as compounds **13**, **16**, **28** and **29**) cannot completely compete with it, despite their high inhibition potency. This was already observed for the earlier described compound **9** [23]. In contrast, the covalent irreversible inhibitor JZL-184 **1** can fully compete with the probe, as demonstrated by the nearly fully disappeared MAGL bands in the presence of 1 μM JZL-184. The serine hydrolase bands associated with other enzymes showed a reduced band intensity or disappeared fully according to the tested control inhibitors (Fig. 5): the FAAH band with URB597, the ABHD6 band with WWL70 and THL, and the ABHD12 band with THL. In the case of pre-treatment with MAFP, all the bands relative to FAAH, MAGL, ABHD6, and ABHD12 showed a strong reduction of band intensity or disappeared completely (Fig. 5).

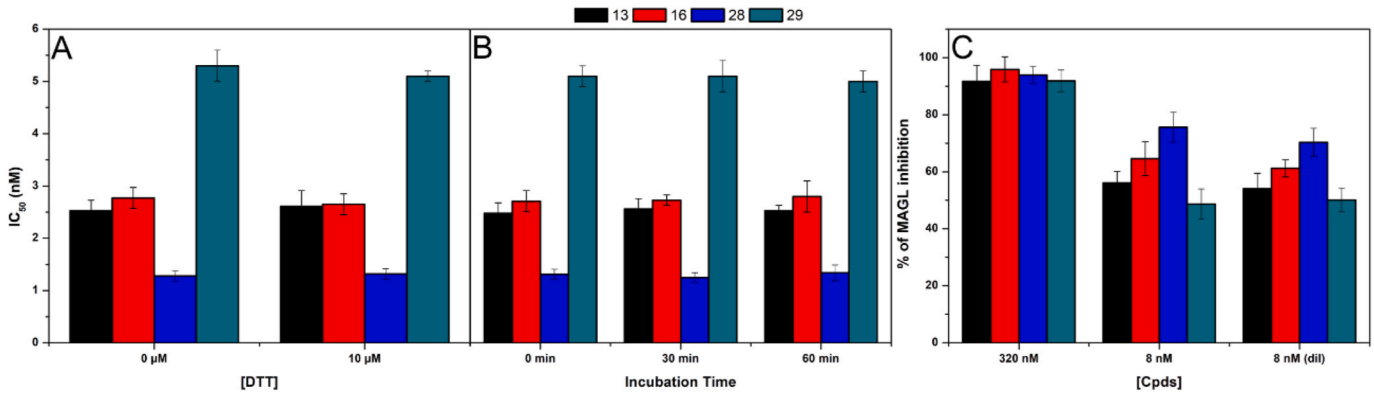

Fig. 3. Analysis of the mechanism of MAGL inhibition of compounds **13**, **16**, **28** and **29**. A) Effect of DTT on MAGL inhibition activity. B) IC_{50} (nM) values at different pre-incubation times with MAGL (0 min, 30 min and 60 min). C) Dilution assay: the first two columns indicate the inhibition percentage of the compound at a concentration of 320 nM and 8 nM. The third column indicates the inhibition percentage of the compound after dilution (final concentration = 8 nM).

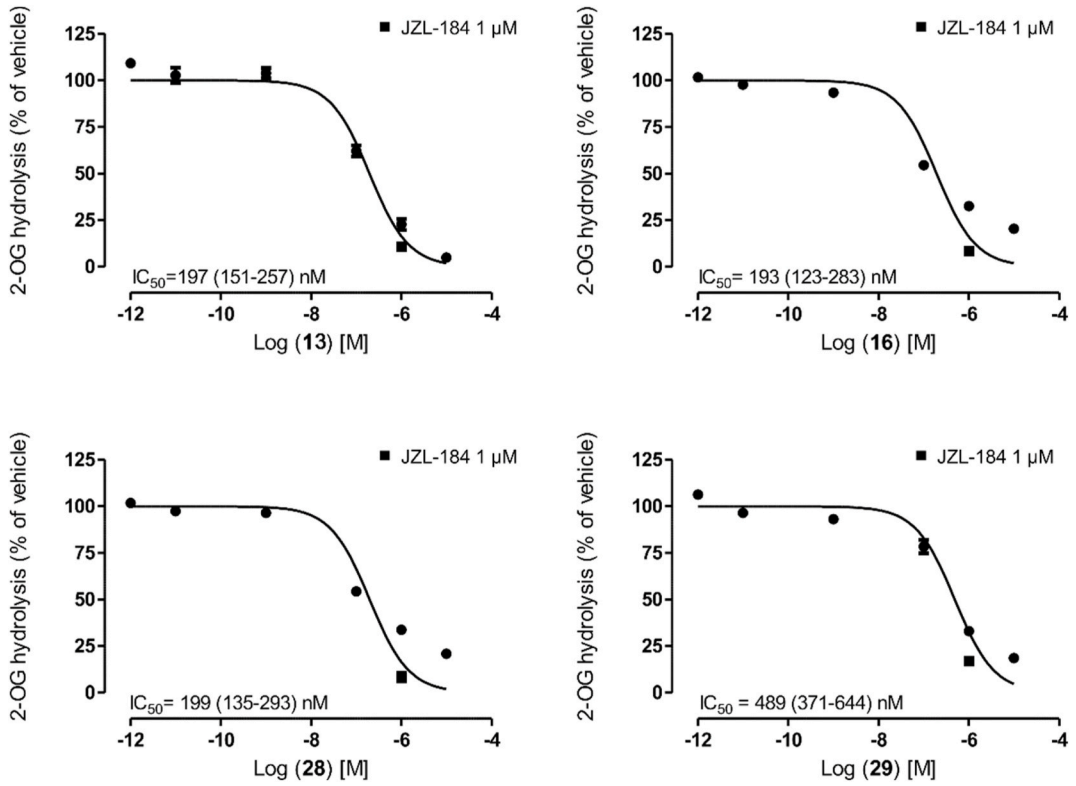

Fig. 4. Concentration-dependent inhibition of 2-oleoylglycerol (2-OG) hydrolysis in intact U937 cells for compounds **13**, **16**, **28** and **29**. Compounds were co-incubated with cells for 30 min and then 10 μM of 2-OG with a 1.0 nM of [^{3}H]2-OG as tracer was added to the cells for additional 5 min at 37 °C. JZL-184 (1 μM) was used as a positive control for full inhibition of MAGL. Data represent mean ± SD of two independent experiments performed with triplicates. IC_{50} values are expressed as mean (95 % CI).

2.6. *In vitro* ADME-tox properties

In vitro ADME properties were assessed for the best MAGL inhibitor of this series, compound **28**, and its piperazine-containing analogue **29**, in comparison with the previously published benzoylpiperidine derivative **8** [22], and the results are reported in the following Table 2. Compounds **28** and **29** have improved thermodynamic aqueous solubility values (3.213 ng/mL, and 5466.541 ng/mL, respectively) with respect to the reference compound **8** (0.129 ng/mL). It is noteworthy to observe that the presence of a piperazine ring in **29** instead of the piperidine group of **28** led to a marked increase (about 1700-fold improvement) in the aqueous solubility property. Parallel artificial membrane permeability assay (PAMPA) was performed to evaluate the ability of these compounds to pass through a biological membrane and reach the target. Compounds **28** and **29** present permeability values comparable to that of the reference compound, with a significant reduction of the membrane retention rates, that are 17.3 % for **28** and 3.2 % for **29** compared to 47.0 % of reference compound **8**. Stability test was performed at 37 °C in human plasma for 24 h: **29** showed to be stable for more than 24 h, while **28** exhibited reduced stability of 74.13 %, turning out to be more susceptible to the metabolic reactions occurring at the plasma level. Finally, the two new compounds provided excellent metabolic stability values in human liver microsomes (96.76 % for **28** and 98.51 % for **29**), greater than that of reference compound **8** (90.71 %).

Median Lethal dose (LD_{50}) has been determined for the two newly

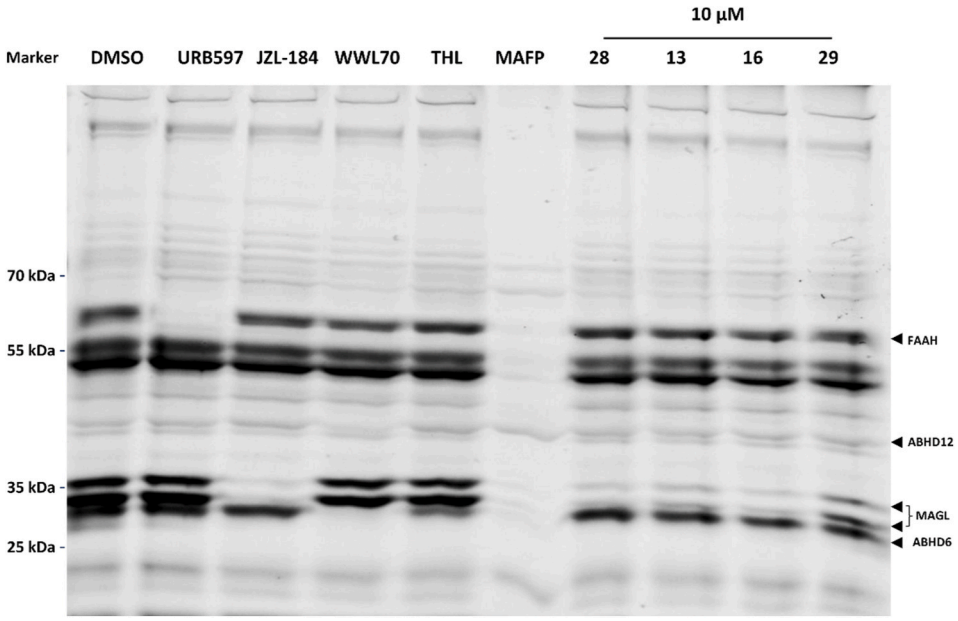

Fig. 5. ABPP with fluorescent labeling of serine hydrolases in mouse brain membrane homogenates using a TAMRA-FP serine hydrolase probe and different inhibitors as controls. The mouse brain membranes (2 mg/mL) were pre-incubated for 25 min with either DMSO, compounds **13**, **16**, **28** and **29** (10 μM, MAGL inhibitors), JZL-184 **1** (1 μM, MAGL inhibitor), URB597 (4 μM, FAAH inhibitor), WWL70 (10 μM, ABHD6 inhibitor), THL (20 μM, ABHD6 and ABHD12 inhibitor) or MAFP (5 μM, unselective serine hydrolase inhibitor). After additional incubation with TAMRA-FP (125 nM) for 5 min, the samples were separated in a SDS-PAGE. A representative image of the TAMRA-FP signal after SDS-PAGE is shown. The presented results could be observed in 3 independent experiments.

Table 2
In vitro ADME assays of compounds **28** and **29**, in comparison with compound **8**.

Compound	Water Solubility ng/mL (LogS)	P_{app} x 10^{-6} cm/s (RM %)	Metabolic Stability %	Stability in human plasma after 24 h %
8	0.129 (−9.588)	1.827 (47.0)	90.71	>99
28	3.213 (−7.649)	3.296 (17.3)	96.76	74.13
29	5466.541 (−4.953)	1.326 (3.2)	98.51	>99

synthesized compounds in *Tenebrio molitor* coleoptera (TMC) toxicity model [35]. After the range-finding study, 1 μL of compound has been administered to five TMC, at a single dose of 200 mg/kg, and vitality observed for seven days. The protocol has been repeated until LD_{50} was determined, and finally confirmed with ten TMC. The LD_{50} for **28** was 200 mg/kg of body weight, while **29** resulted to be safer, with a LD_{50} value of 300 mg/kg (Fig. 6). In conclusion, compound **29** represents the most promising compound of the series, with a good compromise between solubility and passive permeability, and excellent stability and *in vivo* safety.

2.7. Molecular modeling studies

Compound **28** and its piperazine analogue **29**, the most promising derivatives of this new class of MAGL inhibitors, were subjected to molecular modeling studies with the aim of predicting their potential binding mode into MAGL binding site. The ligands were docked into the X-ray structure of MAGL (PDB code 5ZUN) [21] using the robust protocol based on AUTODOCK4 software used in our previous study [23]. The most energetically favored ligand-protein complex predicted by the docking procedure for each ligand was then subjected to a μs-long molecular dynamics (MD) simulation to refine the bioactive conformations predicted for the two compounds (see Experimental section for details). Fig. 7 shows the minimized average structures of MAGL in complex with **28** (Figs. 7A) and **29** (Fig. 7B) in their MD-refined binding conformation, generated from the last 0.5 μs of MD simulation. The ligands assume a similar U-shaped conformation, with the benzoylpiperidine/piperazine core placed within the portion of MAGL binding site including the oxyanion hole, the *m*-disubstituted central phenyl ring properly fitting the curvature of the binding pocket adjacent to its entrance, and the terminal *p*-trifluoromethylpyridine moiety partially protruding outside the cavity and blocking its access. Both compounds form a strong and stable triad of H-bond interactions, maintained for more than 90 % of the MD simulation, which firmly anchor them to the catalytic region of MAGL binding site. In particular, the carbonyl groups of the ligands show two H-bonds with the backbone NH groups of A51 and M123, whereas the third H-bond is established with H121 by the terminal phenolic group of the ligands. Moreover, the *p*-fluorophenolic rings of the two compounds form hydrophobic interactions mainly with the side chains of A51, E53, I179, L184 and V270. The slight difference in the binding modes of the two ligands arises, as expectable, from the presence of the additional nitrogen in the piperazine ring of **29**, with respect to the piperidine core of **28**. In fact, besides showing hydrophobic interactions with L148, I179 and L241, also shared with **28**, the positively charged nitrogen of **29** forms a stable water-bridged H-bond with the backbone oxygen of L241 that is maintained for most of the MD simulation (Fig. 7B). The presence of a structural water molecule between L241 and the piperazine ring of **29** determines a shift of the diarylsulfide fragment of the molecule, compared with the disposition assumed by the same fragment of **28**. In particular, the *m*-disubstituted phenyl ring of **28** predominantly interact only with the side chain of L241 through lipophilic interactions, whereas the terminal *p*-trifluoromethylpyridine group of the ligand is enclosed among D180, V183, R240, and L241, showing hydrophobic contacts with these residues that form a sort of neck at the entrance of MAGL binding site (Fig. 7A). Differently, the diarylsulfide fragment of **29** is shifted toward L205; therefore, the *m*-disubstituted phenyl ring of **29** forms extensive interactions with L205 and L241, between which it is sandwiched, while the ligand *p*-trifluoromethylpyridine ring is slightly more buried within the binding cavity and less solvent-exposed, compared to**28**, but shows hydrophobic contacts only with I179, D180 (Fig. 7B). Despite these small differences,

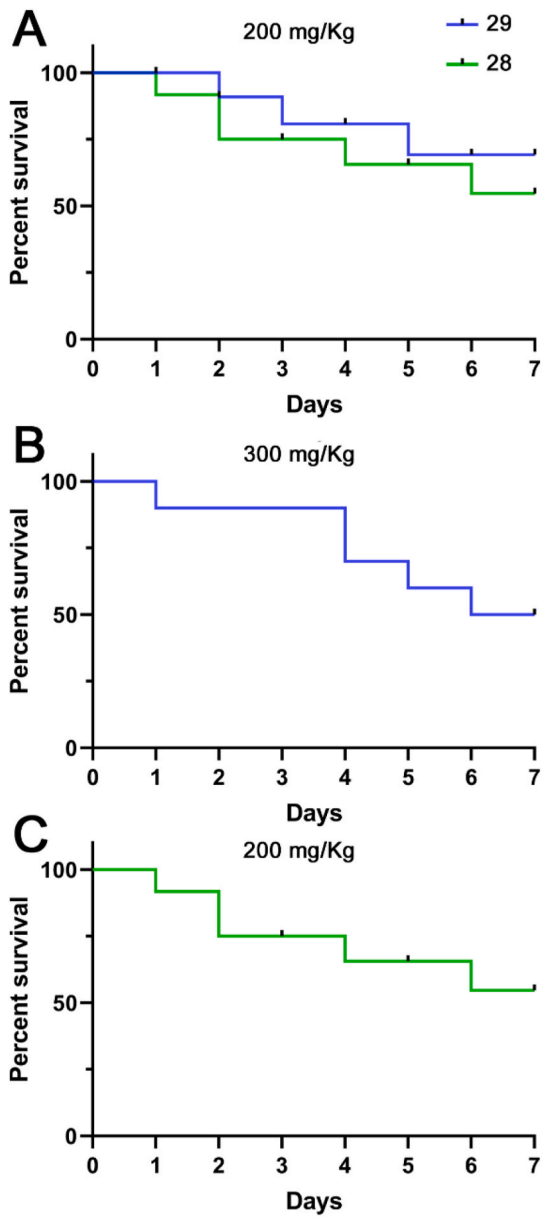

Fig. 6. Kaplan-Meier survival rate curve for compounds **28** and **29** after a single dose administration at the dose of 200 mg/kg (A); Kaplan-Meier survival rate curve for compound **29** after a single dose administration at the dose of 300 mg/kg (B); Kaplan-Meier survival rate curve for compound **28** after a single dose administration at the dose of 200 mg/kg (C).

the overall binding disposition and the pattern of interactions predicted for the two MAGL inhibitors is similar, with the obvious exception of the water-bridged H-bond formed by **29**, which cannot be formed by **28**. We believe that the presence of this additional stable interaction formed by **29**, which should clearly improve the affinity of the ligand for the enzyme, can partially compensate for the considerable energetic penalty associated to the desolvation of the positively charged moiety in the ligand, which is instead deleterious for the activity of the compound. In fact, in absence of such interaction, the decrease in activity of **29** with respect to **28** due to the desolvation effect would expectedly be much higher. In conclusion, the binding features predicted for **28** and **29** can justify the MAGL inhibitory activities determined for the two analogues. In addition, we also found that the binding mode predicted for **28** closely resembles that predicted for the reference compound **9** (Fig. S55). Nevertheless, the presence of the sulfide linker in place of the oxygen seems to allow an orientation of the *p*-trifluoromethylpyridine ring of compound **28** that better fits the entrance of MAGL binding site, maximizing the interactions with D180, V183, R240, and L241 (Fig. 7A), and potentially justifying its increased activity compared to **9**.

Based on these analyses, it is also possible to better rationalize some SAR data observed in the experimental assays. The replacement of the fluorine atom in the phenolic ring with bulkier substituents, as in the case of compounds **22** and **25**, results in a reduction of the inhibitory activity. This effect could be justified by the steric hindrance of these substituents, which would collide with the surrounding protein residues, mainly A51 and I179, thus preventing the proper disposition of the ligand and the formation of its key H-bond interactions. For the same reason, the presence of bulky substituents in the *ortho* position to the phenolic OH group as in compounds **24** and **27**, would not permit the stabilization of the H-bond with H121, which is crucial to strongly anchor the ligand to the binding site of the enzyme, thus justifying the reduced activity of the two compounds. Moreover, we believe that the presence of a methoxy substituent on the central phenyl ring in compounds **18** and **19** could impair the binding mode of the ligand respectively altering the relative disposition of the trifluoromethylpyridine moiety, increasing its exposure to the solvent, and generating a steric clash with L241. Finally, the reduced activity associated to the shift of the trifluoromethyl group on the pyridine ring could be due to either an increased exposure to the solvent of the substituent (as for **12**) or a steric clash with D189 and V183 (as for **14** and **15**).

3. Conclusions

In this work, we aimed to optimize the benzylpiperidine-based MAGL inhibitors previously described and here exemplified by compound **9** [23], as a new scaffold in the field of reversible MAGL inhibitors. Different chemical modifications were introduced to improve MAGL inhibition potency of the new compounds, leading to benzylpiperidine **13**, **16**, **28** and benzylpiperazine **29** which showed IC_{50} values in the 1.3–5.2 nM range on the isolated enzyme. These compounds were further analyzed in intact U937 cells to mimic a more physiological system to evaluate MAGL inhibition and all of them maintained the ability to block MAGL. The four compounds exhibited an excellent MAGL selectivity compared to other serine hydrolyses including ECS enzymes (ABHD6, ABHD12 and FAAH) and CB1 and CB2 receptors, as confirmed by binding and cell-based enzymatic assays and ABPP experiments. We observed a slight decrease in MAGL inhibition potency for the benzylpiperazine derivative **29**, however this fact was adequately compensated for by improved ADME properties, such as increased aqueous solubility, reduced membrane retention rate and greater stability both in human plasma and liver microsomes. In addition, compound **29** proved to be safer compared to its benzylpiperidine analogue **28**, displaying a higher LD_{50} in a *Tenebrio molitor* coleoptera toxicity model. Molecular modeling studies revealed, as expected, a very similar interaction with MAGL for the two compounds and the presence in compound **29** of a piperazine ring (replaced by a piperidine ring in **28**) allowed the establishment of a stable water-bridged H-bond between the positively charged nitrogen atom of **29** and the backbone oxygen atom of L241, thus provoking a shift of the diarylsulfide fragment of **29**. Taken together, our findings suggest that benzylpiperazine-based compound **29** can be further developed for the discovery of reversible MAGL inhibitors, and future work will be focused on structural fine tuning of this chemical scaffold.

4. Experimental section

4.1. Synthesis. General procedures and materials

All solvents and chemicals were used as purchased without further purification. Chromatographic separations were performed on silica gel columns by flash chromatography (Kieselgel 40, 0.040−0.063 mm; Merck). Reactions were followed by thin layer chromatography (TLC) on

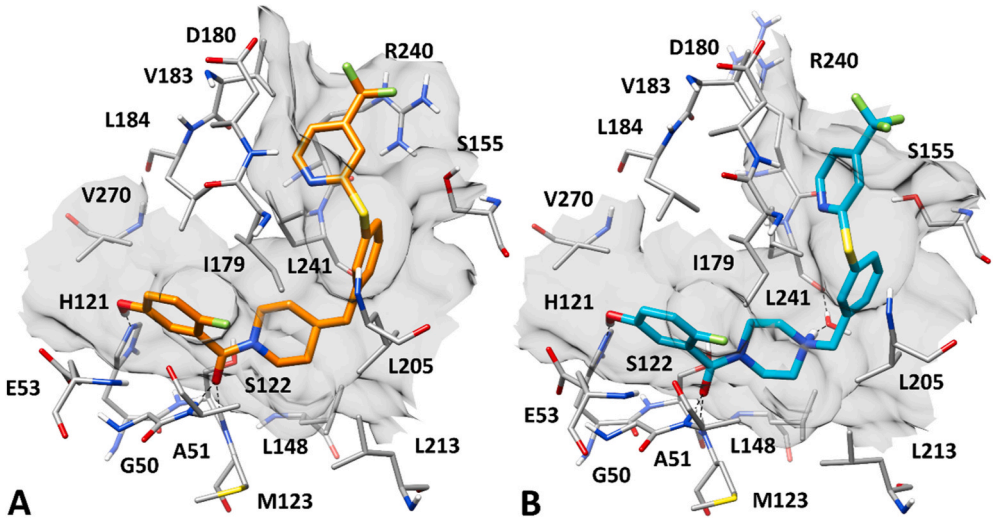

Fig. 7. Minimized average structure of *h*MAGL in complex with compound **28** (A) and **29** (B) in their predicted binding pose after MD simulation. The protein residues surrounding the ligands, as well as the inner surface of the protein binding site, are shown in grey. Direct and water-bridged ligand-protein hydrogen bonds are highlighted as black dashed lines.

Merck aluminum silica gel (60 F254) sheets that were visualized under a UV lamp. Evaporation was performed *in vacuo* (rotating evaporator). Sodium sulfate was always used as the drying agent. Proton (^{1}H) and carbon (^{13}C) NMR spectra were obtained with a Bruker Avance III 400 MHz spectrometer using the indicated deuterated solvents. Chemical shifts are given in parts per million (ppm) (δ relative to residual solvent peak for ^{1}H and ^{13}C). ^{1}H NMR spectra are reported in this order: multiplicity and number of protons. Standard abbreviation indicating the multiplicity were used as follows: s = singlet, d = doublet, dd = doublet of doublets, ddd = doublet of doublet of doublets, t = triplet, tt = triplet of triplets, dt = doublet of triplets, td = triplet of doublets, q = quartet, m = multiplet, bm = broad multiplet and bs = broad singlet. HPLC analysis was used to determine purity: all target compounds (i.e., assessed in biological assays) were ≥95 % pure by HPLC, as confirmed via UV detection (λ = 254 nm). Analytical reversed-phase HPLC was conducted using a Kinetex EVO C18 column (5 μm, 150 × 4.6 mm, Phenomenex, Inc.); eluent A, water; eluent B, CH_3CN; after 5 min at 25 % B, a gradient was formed from 25 % to 75 % of B in 5 min and held at 75 % of B for 10 min; flow rate was 1 mL/min. HPLC analyses were performed at 254 nm. The ESI-MS spectra were recorded by direct injection at a 5 μL min^{-1} flow rate in an Orbitrap high-resolution mass spectrometer (Thermo, San Jose, CA, USA), equipped with a HESI source. The working conditions were as follows: positive polarity, spray voltage of 3.4 kV, capillary temperature of 290 °C, S-lens RF level 50. The sheath and the auxiliary gases were set at 24 and 5 (arbitrary units), respectively. For acquisition and analysis, Xcalibur 4.2 software (Thermo) was used. For spectra acquisition, a nominal resolution (at *m/z* 200) of 140 000 was used. Compound **88** was synthesized as previously reported [22].

4.1.1. General procedure for the synthesis of compounds 39–46, 93

Commercially available 3-bromothiophenol **34**, 5-bromo-2-fluorothiophenol **35**, 3-bromo-4-fluorothiophenol **36**, 5-bromo-2-methoxythiophenol **37**, 3-bromo-4-methoxythiophenol **38** or synthesized intermediate **92** (200 mg, 1 equiv) and 2-chloro-3-trifluoromethylpyridine **30**, 2-chloro-4-trifluoromethylpyridine **31**, 2-chloro-5-trifluoromethylpyridine **32** or 2-chloro-6-trifluoromethylpyridine **33**, (1 equiv) were mixed in anhydrous DMF (2.7 mL) and treated with anhydrous potassium carbonate (2 equiv). The mixture was stirred at 110 °C overnight, then cooled at room temperature and partitioned between water and ethyl acetate. The organic layer was separated, dried over sodium sulfate, filtered and concentrated. Silica gel column chromatography (1–5% EtOAc in *n*-hexane or petroleum ether) afforded the desired compounds.

2-((3-Bromophenyl)thio)-3-(trifluoromethyl)pyridine (**39**). Light yellow oil, 79 % yield from **30** and **34**. ^{1}H NMR ($CDCl_3$) δ (ppm): 7.15 (ddd, 1H, J = 7.8, 5.0, 0.8 Hz), 7.28 (t, 1H, J = 7.9 Hz), 7.48 (ddd, 1H, J = 7.8, 1.7, 1.1 Hz), 7.54 (ddd, 1H, J = 8.0, 1.9, 1.0 Hz), 7.70 (t, 1H, J = 1.8 Hz), 7.89 (ddd, 1H, J = 7.9, 1.7, 0.6 Hz), 8.44–8.49 (m, 1H).

2-((3-Bromophenyl)thio)-4-(trifluoromethyl)pyridine (**40**). Colourless oil, 99 % yield from **31** and **34**. ^{1}H NMR ($CDCl_3$) δ (ppm): 7.16–7.20 (m, 1H), 7.22–7.26 (m, 1H), 7.34 (t, 1H, J = 7.9 Hz), 7.53 (dt, 1H, J = 8.3, 1.1 Hz), 7.60 (ddd, 1H, J = 8.0, 1.8, 1.0 Hz), 7.77 (t, 1H, J = 1.8 Hz), 8.59 (d, 1H, J = 5.1 Hz).

2-((3-Bromophenyl)thio)-5-(trifluoromethyl)pyridine (**41**). Yellow oil, 81 % yield from **32** and **34**. ^{1}H NMR ($CDCl_3$) δ (ppm): 7.02 (d, 1H, J = 8.5 Hz), 7.34 (t, 1H, J = 7.9 Hz), 7.54 (ddd, 1H, J = 7.8, 1.6, 1.0 Hz), 7.61 (ddd, 1H, J = 8.0, 1.9, 1.0 Hz), 7.69 (dd, 1H, J = 8.5, 1.9 Hz), 7.77 (t, 1H, J = 1.7 Hz), 8.63–8.69 (m, 1H).

2-((3-Bromophenyl)thio)-6-(trifluoromethyl)pyridine (**42**). Yellow oil, 73 % yield from **33** and **34**. ^{1}H NMR ($CDCl_3$) δ (ppm): 7.06 (d, 1H, J = 8.2 Hz), 7.33 (t, 1H, J = 7.9 Hz), 7.39 (dd, 1H, J = 7.7, 0.6 Hz), 7.56 (ddd, 1H, J = 7.8, 1.7, 1.0 Hz), 7.59 (ddd, 1H, J = 8.0, 1.9, 1.1 Hz), 7.64 (td, 1H, J = 7.9 Hz), 7.79 (t, 1H, J = 1.8 Hz).

2-((5-Bromo-2-fluorophenyl)thio)-4-(trifluoromethyl)pyridine (**43**). Light yellow oil, 67 % yield from **31** and **35**. ^{1}H NMR ($CDCl_3$) δ (ppm): 7.11 (t, 1H, J = 8.5 Hz), 7.23–7.29 (m, 2H), 7.58 (ddd, 1H, J = 8.7, 4.4, 2.5 Hz), 7.75 (dd, 1H, J = 6.1, 2.5 Hz), 8.55 (d, 1H, J = 5.0 Hz).

2-((3-Bromo-4-fluorophenyl)thio)-4-(trifluoromethyl)pyridine (**44**). Light yellow oil, 62 % yield from **31** and **36**. ^{1}H NMR ($CDCl_3$) δ (ppm): 7.16–7.21 (m, 1H), 7.21–7.26 (m, 2H), 7.50–7.56 (m, 1H), 7.83 (dd, 1H, J = 6.4, 2.0 Hz), 8.56 (d, 1H, J = 5.2 Hz).

2-((5-Bromo-2-methoxyphenyl)thio)-4-(trifluoromethyl)pyridine (**45**). Colourless oil, 65 % yield from **31** and **37**. ^{1}H NMR ($CDCl_3$) δ (ppm): 3.78 (s, 3H), 6.89 (d, 1H, J = 8.8 Hz), 7.08–7.11 (m, 1H), 7.20 (dd, 1H, J = 5.1, 0.8 Hz), 7.56 (dd, 1H, J = 8.8, 2.5 Hz), 7.72 (d, 1H, J = 2.5 Hz), 8.56 (d, 1H, J = 5.2 Hz).

2-((3-Bromo-4-methoxyphenyl)thio)-4-(trifluoromethyl)pyridine (**46**). Light yellow oil, 79 % yield from **31** and **38**. ^{1}H NMR ($CDCl_3$) δ (ppm): 3.96 (s, 3H), 6.98 (d, 1H, J = 8.6 Hz), 7.05–7.09 (m, 1H), 7.17–7.20 (m, 1H), 7.53 (dd, 1H, J = 8.5, 2.2 Hz), 7.80 (d, 1H, J = 2.2 Hz), 8.56 (d, 1H, J = 5.1 Hz).

Methyl 3-((4-(trifluoromethyl)pyridin-2-yl)thio)benzoate (**93**). Colourless oil, 60 % yield from **31** and **92**. ^{1}H NMR ($CDCl_3$) δ (ppm): 3.93 (s,

3H), 7.13–7.16 (m, 1H), 7.22 (d, 1H, $J = 5.1$ Hz), 7.55 (t, 1H, $J = 7.8$ Hz), 7.76–7.81 (m, 1H), 8.11–8.15 (m, 1H), 8.26–8.29 (m, 1H), 8.57 (d, 1H, $J = 5.1$ Hz).

4.1.2. General procedure for the synthesis of compounds 47-54

tert-Butyl 4-methylenepiperidine-1-carboxylate (1.25 equiv) in anhydrous toluene (1.6 mL) was treated with 9-BBN (0.5 M in THF, 1.25 equiv), and heated at 115 °C for 1 h. The reaction mixture was cooled, treated with NaOH (3.2 M aqueous solution, 3 equiv) followed by Pd $(PPh_3)_4$ (0.03 equiv). Finally, intermediates **39**–**46** (280 mg, 1 equiv) in anhydrous toluene (0.7 mL) and tetrabutylammonium iodide (0.5 equiv) were added. The reaction mixture was placed under argon and heated at 115 °C. After 18 h, the mixture was cooled and partitioned between EtOAc and saturated aqueous $NaHCO_3$. The organic layer was separated and dried over sodium sulfate, filtered and concentrated to obtain a crude, which was purified by silica gel column chromatography (10–20 % EtOAc in *n*-hexane or petroleum ether) to give the desired products.

tert-Butyl 4-(3-((3-(trifluoromethyl)pyridin-2-yl*)thio)benzyl)piperidine-1-carboxylate* (**47**). Orange oil, 76 % yield from **39.** ^{1}H NMR ($CDCl_3$) δ (ppm): 1.45 (s, 9H), 1.50–1.90 (bm, 5H), 2.56 (d, 2H, $J = 6.9$ Hz), 2.63 (td, 2H, $J = 12.9$, 2.1 Hz), 4.01–4.09 (m, 2H), 7.12 (ddd, 1H, $J = 8.5$, 4.8, 0.6 Hz), 7.16–7.20 (m, 1H), 7.31–7.37 (m, 2H), 7.40 (dt, 1H, $J = 7.6$, 1.5 Hz), 7.88 (dd, 1H, $J = 7.8$, 1.2 Hz), 8.40–8.46 (m, 1H).

tert-Butyl 4-(3-((4-(trifluoromethyl)pyridin-2-yl*)thio)benzyl)piperidine-1-carboxylate* (**48**). Yellow oil, 99 % yield from **40.** ^{1}H NMR ($CDCl_3$) δ (ppm): 1.44 (s, 9H), 1.47–1.93 (bm, 5H), 2.57 (d, 2H, $J = 7.2$ Hz), 2.63 (td, 2H, $J = 12.9$, 2.6 Hz), 4.02–4.14 (m, 2H), 6.99–7.02 (m, 1H), 7.17–7.26 (m, 2H), 7.35–7.43 (m, 2H), 7.46 (dt, 1H, $J = 7.8$, 1.5 Hz), 8.58 (d, 1H, $J = 5.3$ Hz).

tert-Butyl 4-(3-((5-(trifluoromethyl)pyridin-2-yl*)thio)benzyl)piperidine-1-carboxylate* (**49**). Yellow oil, 62 % yield from **41.** ^{1}H NMR ($CDCl_3$) δ (ppm): 1.45 (s, 9H), 1.52–1.75 (bm, 4H), 1.76–1.90 (bm, 1H), 2.58 (d, 2H, $J = 7.0$ Hz), 2.60–2.70 (m, 2H), 4.01–4.13 (m, 2H), 6.92 (d, 1H, $J = 8.4$ Hz), 7.23–7.27 (m, 1H), 7.35–7.50 (m, 3H), 7.64 (dd, 1H, $J = 8.6$, 2.1 Hz), 8.61–8.68 (m, 1H).

tert-Butyl 4-(3-((6-(trifluoromethyl)pyridin-2-yl*)thio)benzyl)piperidine-1-carboxylate (***50**). Amber oil, 80 % yield from **42.** ^{1}H NMR ($CDCl_3$) δ (ppm): 1.45 (s, 9H), 1.50–1.93 (bm, 5H), 2.56 (d, 2H, $J = 7.2$ Hz), 2.64 (td, 2H, $J = 12.9$, 2.3 Hz), 4.02–4.14 (m, 2H), 6.99 (d, 1H, $J = 8.2$ Hz), 7.20–7.25 (m, 1H), 7.32–7.48 (m, 4H), 7.59 (t, 1H, $J = 7.9$ Hz).

tert-Butyl 4-(4-fluoro-3-((4-(trifluoromethyl)pyridin-2-yl*)thio)benzyl) piperidine-1-carboxylate* (**51**). Amber oil, 56 % yield from **43.** ^{1}H NMR ($CDCl_3$) δ (ppm): 1.07–1.21 (bm, 1H), 1.45 (s, 9H), 1.58–1.71 (bm, 2H), 1.78–1.92 (bm, 2H), 2.55 (d, 2H, $J = 7.0$ Hz), 2.56–2.70 (bm, 2H), 4.00–4.18 (bm, 2H), 7.10–7.13 (m, 1H), 7.15 (d, 1H, $J = 8.3$ Hz), 7.19–7.25 (m, 2H), 7.37 (dd, 1H, $J = 6.8$, 2.1 Hz), 8.55 (d, 1H, $J = 5.2$ Hz).

tert-Butyl 4-(2-fluoro-5-((4-(trifluoromethyl)pyridin-2-yl*)thio)benzyl) piperidine-1-carboxylate* (**52**). Yellow oil, 23 % yield from **44.** ^{1}H NMR ($CDCl_3$) δ (ppm): 1.11–1.24 (bm, 2H), 1.45 (s, 9H), 1.48–1.91 (bm, 3H), 2.60 (d, 2H, $J = 7.1$ Hz), 2.62–2.72 (m, 2H), 3.99–4.20 (bm, 2H), 6.98–7.03 (m, 1H), 7.13 (t, 1H, $J = 8.9$ Hz), 7.19 (d, 1H, $J = 4.8$ Hz), 7.37–7.42 (m, 1H), 7.42–7.48 (m, 1H), 8.56 (d, 1H, $J = 5.1$ Hz).

tert-Butyl 4-(4-methoxy-3-((4-(trifluoromethyl)pyridin-2-yl*)thio) benzyl)piperidine-1-carboxylate* (**53**). Colourless oil, 35 % yield from **45.** ^{1}H NMR ($CDCl_3$) δ (ppm): 1.08–1.18 (bm, 2H), 1.45 (s, 9H), 1.56–1.66 (bm, 3H), 2.51 (d, 2H, $J = 7.0$ Hz), 2.58–2.69 (m, 2H), 3.79 (s, 3H), 4.02–4.14 (bm, 2H), 6.95 (d, 1H, $J = 8.4$ Hz), 6.96–6.99 (m, 1H), 7.14–7.18 (m, 1H), 7.24 (dd, 1H, $J = 8.3$, 2.1 Hz), 7.37 (d, 1H, $J = 2.3$ Hz), 8.55 (d, 1H, $J = 5.1$ Hz).

tert-Butyl 4-(2-methoxy-5-((4-(trifluoromethyl)pyridin-2-yl*)thio) benzyl)piperidine-1-carboxylate* (**54**). Amber oil, 49 % yield from **46**. ^{1}H NMR ($CDCl_3$) δ (ppm): 1.45 (s, 9H), 1.46–1.90 (bm, 5H), 2.56 (d, 2H, $J = 7.0$ Hz), 2.60–2.70 (m, 2H), 3.88 (s, 3H), 3.98–4.17 (m, 2H), 6.91–6.96 (m, 2H), 7.15 (dd, 1H, $J = 5.2$, 1.0 Hz), 7.29 (d, 1H, $J = 2.3$ Hz), 7.45 (dd, 1H, $J = 8.4$, 2.3 Hz), 8.56 (d, 1H, $J = 5.2$ Hz).

4.1.3. General procedure for the synthesis of compounds 55–62, 97

N-Boc-piperidine intermediates **47**–**54** or *N*-Boc-piperazine intermediate **96** (280 mg, 1 equiv) were dissolved in methanol (0.9 mL) and dichloromethane (0.9 mL), treated dropwise with HCl (4.0 M in dioxane, 6 equiv) and stirred at room temperature for 1 h. Toluene (1 mL) was added and the reaction mixture was concentrated under nitrogen flux. A second evaporation from toluene (1 mL) followed by high vacuum afforded the title compounds, which were used in the next step without further purification.

2-((3-(Piperidin-4-ylmethyl)phenyl)thio)-3-(trifluoromethyl)pyridine hydrochloride (**55**). Yellow oil. 99 % yield from **47**. ^{1}H NMR (D_2O) δ (ppm): 1.30–1.90 (bm, 5H), 2.59 (d, 2H, $J = 6.6$ Hz), 2.82–2.95 (m, 2H), 3.30–3.42 (m, 2H), 7.27–7.44 (m, 5H), 8.16 (d, 1H, $J = 7.3$ Hz), 8.37–8.40 (m, 1H).

2-((3-(Piperidin-4-ylmethyl)phenyl)thio)-4-(trifluoromethyl)pyridine hydrochloride (**56**). Yellow oil, 99 % yield from **48**. ^{1}H NMR (D_2O) δ (ppm): 1.32–1.88 (bm, 5H), 2.62 (d, 2H, $J = 7.4$ Hz), 2.88 (t, 2H, $J = 12.0$ Hz), 3.31–3.40 (m, 2H), 7.26–7.30 (m, 1H), 7.34–7.51 (m, 5H), 8.52 (d, 1H, $J = 5.6$ Hz).

2-((3-(Piperidin-4-ylmethyl)phenyl)thio)-5-(trifluoromethyl)pyridine hydrochloride (**57**). Yellow oil, 99 % yield from **49**. ^{1}H NMR (D_2O) δ (ppm): 1.37–1.52 (bm, 4H), 1.70–2.00 (bm, 1H), 2.67 (d, 2H, $J = 6.8$ Hz), 2.87–2.99 (m, 2H), 3.36–3.44 (m, 2H), 7.17–7.23 (m, 1H), 7.38–7.57 (m, 4H), 7.91–8.00 (m, 1H), 8.64–8.72 (m, 1H).

2-((3-(Piperidin-4-ylmethyl)phenyl)thio)-6-(trifluoromethyl)pyridine hydrochloride (**58**). Orange oil, 99 % yield from **50**. ^{1}H NMR (D_2O) δ (ppm): 1.27–1.87 (bm, 5H), 2.56 (d, 2H, $J = 6.8$ Hz), 2.78–2.90 (m, 2H), 3.30–3.40 (m, 2H), 6.97–7.17 (m, 2H), 7.25–7.40 (m, 3H), 7.47 (d, 1H, $J = 7.5$ Hz), 7.68 (t, 1H, $J = 7.9$ Hz).

2-((2-Fluoro-5-(piperidin-4-ylmethyl)phenyl)thio)-4-(trifluoromethyl) pyridine hydrochloride (**59**). Yellow oil, 99 % yield from **51**. ^{1}H NMR (D_2O) δ (ppm): 1.30–1.50 (m, 3H), 1.72–1.92 (m, 2H), 2.60 (d, 2H, $J = 6.8$ Hz), 2.84–2.95 (m, 2H), 3.33–3.42 (m, 2H), 7.22 (t, 1H, $J = 8.8$ Hz), 7.32–7.36 (m, 1H), 7.36–7.42 (m, 1H), 7.44–7.50 (m, 2H), 8.50 (d, 1H, $J = 5.3$ Hz).

2-((4-Fluoro-3-(piperidin-4-ylmethyl)phenyl)thio)-4-(trifluoromethyl) pyridine hydrochloride (**60**). Yellow solid, 98 % yield from **52**. ^{1}H NMR (D_2O) δ (ppm): 1.37–2.00 (m, 5H), 2.68 (d, 2H, $J = 7.1$ Hz), 2.86–2.97 (m, 2H), 3.35–3.44 (m, 2H), 7.19–7.30 (m, 2H), 7.46 (d, 1H, $J = 5.7$ Hz), 7.49–7.56 (m, 2H), 8.52 (d, 1H, $J = 5.1$ Hz).

2-((2-Methoxy-5-(piperidin-4-ylmethyl)phenyl)thio)-4-(trifluoromethyl)pyridine hydrochloride (**61**). Yellow oil, 99 % yield from **53**. ^{1}H NMR (D_2O) δ (ppm): 1.38–1.51 (m, 2H), 1.84–1.95 (m, 3H), 2.63 (d, 2H, $J = 6.6$ Hz), 2.90–3.01 (m, 2H), 3.39–3.47 (m, 2H), 3.81 (s, 3H), 7.20 (d, 1H, $J = 8.8$ Hz), 7.27–7.30 (m, 1H), 7.44–7.52 (m, 2H), 7.54 (d, 1H, $J = 5.4$ Hz), 8.57 (d, 1H, $J = 5.2$ Hz).

2-((4-Methoxy-3-(piperidin-4-ylmethyl)phenyl)thio)-4-(trifluoromethyl)pyridine hydrochloride (**62**). Light brown solid, 99 % yield from **54**. ^{1}H NMR (D_2O) δ (ppm): 1.38–2.00 (bm, 5H), 2.65 (d, 2H, $J = 7.1$ Hz), 2.85–2.97 (m, 2H), 3.37–3.45 (m, 2H), 3.93 (s, 3H), 7.15–7.25 (m, 2H), 7.42–7.47 (m, 1H), 7.49–7.54 (m, 1H), 7.55–7.62 (m, 1H), 8.57 (d, 1H. $J = 5.4$ Hz).

1-(3-((4-(Trifluoromethyl)pyridin-2-yl*)thio)benzyl)piperazine hydrochloride* (**97**). Off-white solid, 99 % yield from **96**. ^{1}H NMR (D_2O) δ (ppm): 3.53–3.69 (m, 8H), 4.49 (s, 2H), 7.44–7.47 (m, 1H), 7.50–7.54 (m, 1H), 7.59–7.65 (m, 2H), 7.72–7.78 (m, 2H), 8.54 (d, 1H, $J = 4.5$ Hz).

4.1.4. General procedure for the synthesis of methyl esters 65a-c, 66a,b, 92

Method a. Commercially available 2-bromo-5-methoxybenzoic acid **63a**, 3-bromo-5-methoxybenzoic acid **63b**, 4-bromo-3-methoxybenzoic acid **63c** or 3-sulfanylbenzoic acid **91** (500 mg, 2.16 mmol) was dissolved in 10.9 mL of anhydrous methanol, followed by a dropwise addition of concentrated sulfuric acid (0.02 mL), and the mixture was refluxed until starting material was consumed. The reaction mixture was cooled to room temperature, the solvent was evaporated, the residue was diluted with water and extracted with EtOAc. The organic phase

was washed with saturated sodium bicarbonate aqueous solution, dried and concentrated to afford crude reaction products **65a-c** and **92**, which was submitted to the next step without further purification. Method b. Under argon atmosphere, thionyl chloride (2.5 equiv) was added dropwise to a solution of commercially available 2-amino-5-methoxybenzoic acid **64a** or 3-amino-5-methoxybenzoic acid **64b** (400 mg, 1 equiv) in dry methanol (3.3 mL) cooled in an ice bath, and then the mixture was refluxed at 80 °C until starting material was consumed (TLC). The reaction mixture was cooled to room temperature and then carefully diluted with water and ethyl acetate, and the organic phase was washed with saturated aqueous $NaHCO_3$ solution. The organic layer was dried over Na_2SO_4 and concentrated. Pure methyl esters **66a,b** were obtained and used in the next step without any further purification.

Methyl 2-bromo-5-methoxybenzoate (**65a**). Colorless oil, 81 % yield from 2-bromo-5-methoxybenzoic acid **63a**. ^{1}H NMR ($CDCl_3$) δ (ppm): 3.82 (s, 3H), 3.93 (s, 3H), 6.89 (dd, 1H, J = 8.9, 3.1 Hz), 7.32 (d, 1H, J = 3.1 Hz), 7.53 (d, 1H, J = 8.8 Hz).

Methyl 3-bromo-5-methoxybenzoate (**65b.**). Colorless oil, 98 % yield from 3-bromo-5-methoxybenzoic acid **63b**. ^{1}H NMR ($CDCl_3$) δ (ppm): 3.84 (s, 3H), 3.92 (s, 3H), 7.24 (dd, 1H, J = 1.6, 1.2 Hz), 7.49 (dd, 1H, J = 2.4, 1.2 Hz), 7.76 (dd, 1H, J = 1.8, 1.4 Hz).

Methyl 4-bromo-3-methoxybenzoate (**65c**). Colorless oil, 89 % yield from 4-bromo-3-methoxybenzoic acid **63c**. ^{1}H NMR ($CDCl_3$) δ (ppm): 3.92 (s, 3H), 3.96 (s, 3H), 7.51 (dd, 1H, J = 8.1, 1.4 Hz), 7.55 (d, 1H, J = 1.2 Hz), 7.61 (d, 1H, J = 8.1 Hz).

Methyl 2-amino-5-methoxybenzoate (**66a**). Amber oil, 84 % yield from 2-amino-5-methoxybenzoic acid **64a**. ^{1}H NMR ($CDCl_3$) δ (ppm): 3.76 (s, 3H), 3.88 (s, 3H), 5.42 (exchangeable bs, 2H), 6.63 (d, 1H, J = 8.9 Hz), 6.95 (dd, 1H, J = 8.9, 3.0 Hz), 7.35 (d, 1H, J = 3.0 Hz).

Methyl 3-amino-5-methoxybenzoate (**66b**). Orange oil, 82 % yield from 3-amino-5-methoxybenzoic acid **64b**. ^{1}H NMR ($CDCl_3$) δ (ppm): 3.80 (s, 3H), 3.88 (s, 3H), 6.41 (t, 1H, J = 2.1 Hz), 6.96–7.00 (m, 2H).

Methyl 3-mercaptobenzoate (**92**). Light-yellow liquid, 63 % yield from 3-sulfanylbenzoic acid **91**. ^{1}H NMR ($CDCl_3$) δ (ppm): 3.54 (exchangeable s, 1H), 3.91 (s, 3H), 7.31 (t, 1H, J = 7.8 Hz), 7.45 (d, 1H, J = 7.8 Hz), 8.16 (d, 1H, J = 7.7 Hz), 7.93–7.97 (m, 1H).

4.1.5. General procedure for the synthesis of diarylsulfides 67a-c

A sealed vial was charged with anhydrous K_2CO_3 (1 equiv), compounds **65a-c** (515 mg, 1 equiv), Pd_2 (dba)$_3$ (0.2 equiv), Xantphos (0.22 equiv), anhydrous toluene (31.5 mL for 2.10 mmol of starting material), and commercially available thiophenol (1.85 equiv). After purging with argon, the vial was closed and the resulting mixture was then heated at 120 °C for 24 h. After cooling to room temperature, the mixture was filtered through a small pad of Celite, washed with ethyl acetate and concentrated under vacuum. The crude product was purified by silica gel chromatography (eluent mixtures of *n*-hexane/petroleum ether with 5–10 % EtOAc) to afford the expected products **67a-c**.

Methyl 5-methoxy-2-(phenylthio)benzoate (**67a**). Yellow oil, 99 % yield from **65a**. ^{1}H NMR ($CDCl_3$) δ (ppm): 3.81 (s, 3H), 3.93 (s, 3H), 6.85–6.93 (m, 1H), 7.30–7.40 (m, 4H), 7.43–7.52 (m, 3H).

Methyl 3-methoxy-5-(phenylthio)benzoate (**67b**). Yellow oil, 99 % yield from **65b**. ^{1}H NMR ($CDCl_3$) δ (ppm): 3.79 (s, 3H), 3.89 (s, 3H), 6.98 (dd, 1H, J = 2.5, 1.7 Hz), 7.15–7.43 (m, 6H), 7.59 (t, 1H, J = 1.5 Hz).

Methyl 3-methoxy-4-(phenylthio)benzoate (**67c**). Yellow oil, 99 % yield from **65c**. ^{1}H NMR ($CDCl_3$) δ (ppm): 3.89 (s, 3H), 3.97 (s, 3H), 6.78 (d, 1H, J = 8.1 Hz), 7.40–7.44 (m, 3H), 7.46–7.49 (m, 1H), 7.50–7.54 (m, 3H).

4.1.6. General procedure for the synthesis of benzoic acids 68a-c, 70a,b

Methyl esters **67a-c**, **69a,b** (855 mg, 3.12 mmol) were dissolved in a 1:1 *v/v* mixture of THF/methanol (31 mL) and treated with 9.4 mL of 2 N aqueous solution of LiOH. The reaction was stirred overnight at room temperature, the solvents were evaporated and the residue was treated with 1 N aqueous HCl and extracted with EtOAc. The organic phase was dried and evaporated to afford the pure desired carboxylic acid derivatives.

5-Methoxy-2-(phenylthio)benzoic acid (**68a**). Orange solid, 70 % yield from **67a**. ^{1}H NMR ($CDCl_3$) δ (ppm): 3.83 (s, 3H), 6.89–6.96 (m, 2H), 7.35–7.42 (m, 3H), 7.45–7.50 (m, 2H), 7.64 (dd, 1H, J = 2.3, 1.0 Hz).

3-Methoxy-5-(phenylthio)benzoic acid (**68b**). Yellow solid, 61 % yield from **67b**. ^{1}H NMR ($CDCl_3$) δ (ppm): 3.80 (s, 3H), 7.01 (dd, 1H, J = 2.5, 1.7 Hz), 7.29–7.38 (m, 3H), 7.40–7.45 (m, 3H), 7.61 (t, 1H, J = 1.5 Hz).

3-Methoxy-4-(phenylthio)benzoic acid (**68c**). Orange solid, 99 % yield from **67c**. ^{1}H NMR ($CDCl_3$) δ (ppm): 3.98 (s, 3H), 6.76 (dd, 1H, J = 8.5 Hz), 7.40–7.46 (m, 3H), 7.50–7.57 (m. 4H).

2-Benzamido-5-methoxybenzoic acid (**70a**). White solid, 76 % yield from **69a**. ^{1}H NMR (acetone-d_6) δ (ppm): 3.87 (s, 3H), 7.29 (dd, 1H, J = 9.2, 3.1 Hz), 7.54–7.65 (m, 3H), 7.68 (d, 1H, J = 3.1 Hz), 7.99–8.06 (m, 2H), 8.89 (d, 1H, J = 9.2 Hz), 12.03 (exchangeable bs, 1H).

3-Benzamido-5-methoxybenzoic acid (**70b**). White solid, 99 % yield from **69b**. ^{1}H NMR (acetone-d_6) δ (ppm): 3.88 (s, 3H), 7.31-0.734 (m, 1H), 7.49–7.56 (m, 2H), 7.60 (t, 1H, J = 7.4 Hz), 7.92 (t, 1H, J = 2.0 Hz), 8.01–8.06 (m, 2H), 8.07–8.11 (m, 1H), 9.68 (exchangeable bs, 1H).

4.1.7. Procedure for the synthesis of 4-benzamido-3-hydroxybenzoic acid (72)

To a suspension of 4-amino-3-hydroxybenzoic acid **71** (80 mg, 1 equiv) in anhydrous THF (1 mL) was added anhydrous pyridine (1.06 equiv) followed by benzoyl chloride (1.05 equiv) at 0 °C. After 5 min, the reaction was quenched with water, then repeatedly extracted with EtOAc, and the combined organic layers were dried over Na_2SO_4. Filtration and then evaporation of the solvent afforded 4-benzamido-3-hydroxybenzoic acid **72** as an orange solid (99 % yield). The product was carried over to next step without further purification. ^{1}H NMR (CD_3OD) δ (ppm): 7.50–7.65 (m, 5H), 7.93–7.98 (m, 2H), 8.17 (d, 1H, J = 8.9 Hz).

4.1.8. General procedure for the synthesis of compounds 27, 69a,b, 74–87, 89, 90, 98

HATU (1.05 equiv) was added to a solution of the appropriate commercially available or in-house synthesized benzoic acid (benzoic acid for **69a,b**; 3-methoxybenzoic acid **73b** for **74**–**81**; 2-fluoro-5-methoxybenzoic acid **73a** for **87** and **98**; 3-((2-methoxyethoxy) methoxy)benzoic acid **88** for **89** and **90**; **68a** for **82**; **68b** for **83**; **68c** for **84**; **70a** for **85**; **70b** for **86**; **72** for **27**; 1 equiv) in dry DMF (3.2 mL), then DIPEA (4 equiv) was added dropwise. The resulting mixture was stirred at room temperature for 30 min, and then piperidine hydrochlorides **55**–**62**, amines **66a,b** or piperazine hydrochloride **97** (270 mg, 1 equiv) were added and left under stirring at room temperature until consumption of starting material (TLC). After this time, the residue was diluted with water and extracted with EtOAc. The organic layer was repeatedly washed with brine, dried over Na_2SO_4, and the solvent was removed under reduced pressure. The residue was purified with a flash column chromatography (silica gel, mixtures from 7:3 to 4:6 of *n*-hexane or petroleum ether/ethyl acetate, or 99:1 $CHCl_3$/ethyl acetate) and pure fractions containing the desired compounds were evaporated to dryness affording the pure amides. In some cases (for compounds **89** and **90**), the obtained crude products were not purified and were submitted to the subsequent step without further analysis.

N-(2-Hydroxy-4-(4-(3-((4-(trifluoromethyl)pyridin-2-yl*)thio)benzyl) piperidine-1-carbonyl)phenyl)benzamide* (**27**). Light red solid, 17 % yield from **56** and **72**. ^{1}H NMR (DMSO-d_6) δ (ppm): 1.08–1.27 (bm, 2H), 1.50–1.68 (bm, 2H), 1.76–1.88 (bm, 1H), 2.61 (d, 2H, J = 6.9 Hz), 2.70–3.06 (bm, 2H), 3.60–3.77 (bm, 1H), 4.30–4.47 (bm, 1H), 6.82 (dd, 1H, J = 8.1, 1.6 Hz), 6.90 (d, 1H, J = 1.8 Hz), 7.09–7.12 (m, 1H), 7.36–7.40 (m, 1H), 7.45–7.50 (m, 3H), 7.50–7.57 (m, 3H), 7.61 (tt, 1H, J = 7.2, 2.0 Hz), 7.79 (d, 1H, J = 8.2 Hz), 7.94–8.00 (m, 2H), 8.66 (d, 1H, J = 5.2 Hz), 9.51 (exchangeable bs, 1H). ^{13}C NMR (DMSO-d_6) δ (ppm): 37.53, 41.57, 114.27, 115.44, 115.70, 117.53, 122.57 (q, J = 274.7 Hz), 126.99, 127.56, 127.98, 128.38, 128.60, 130.12, 130.85, 131.86, 132.60, 133.23, 134.30, 135.66, 137.42, 142.45, 148.92,

151.29, 162.83, 164.64, 165.24, 168.58, 170.40. HPLC analysis: retention time = 13.871 min; peak area, 95 % (254 nm). HRMS: *m/z* for $C_{32}H_{29}F_3N_3O_3S$ $[M + H]^+$ calculated: 592.18817, found: 592.18707.

Methyl 2-benzamido-5-methoxybenzoate (**69a**). Yellow solid, 35 % yield from benzoic acid and **66a**. ^{1}H NMR ($CDCl_3$) δ (ppm): 3.85 (s, 3H), 3.97 (s, 3H), 7.19 (dd, 1H, J = 9.3, 3.1 Hz), 7.48–7.57 (m, 3H), 7.58 (d, 1H, J = 3.1 Hz), 8.01–8.07 (m, 2H), 8.83 (d, 1H, J = 9.3 Hz), 11.79 (exchangeable bs, 1H).

Methyl 3-benzamido-5-methoxybenzoate (**69b**). Amber oil, 83 % yield from benzoic acid and **66b**. ^{1}H NMR ($CDCl_3$) δ (ppm): 3.88 (s, 3H), 3.91 (s, 3H), 7.34–7.37 (m, 1H), 7.47–7.53 (m, 2H), 7.57 (t, 1H, J = 7.2 Hz), 7.65–7.68 (m, 1H), 7.81 (t, 1H, J = 2.0 Hz), 7.85–7.90 (m, 2H), 7.94 (exchangeable bs, 1H).

(3-Methoxyphenyl) (4-(3-((3-(trifluoromethyl)pyridin-2-yl*)thio) benzyl)piperidin*-1-yl*)methanone* (**74**). Colorless oil, 48 % yield from **55** and 3-methoxybenzoic acid **73b**. ^{1}H NMR ($CDCl_3$) δ (ppm): 1.56–1.90 (bm, 5H), 2.59 (d, 2H, J = 6.9 Hz), 2.64–3.00 (bm, 2H), 3.60–3.87 (bm, 1H), 3.82 (s, 3H), 4.54–4.83 (bm, 1H), 6.88–6.96 (m, 3H), 7.12 (dd, 1H, J = 7.9, 4.7 Hz), 7.16–7.21 (m, 1H), 7.27–7.37 (m, 3H), 7.40 (dt, 1H, J = 7.9, 1.4 Hz), 7.88 (dd, 1H, J = 7.8, 1.1 Hz), 8.39–8.44 (m, 1H).

(3-Methoxyphenyl) (4-(3-((4-(trifluoromethyl)pyridin-2-yl*)thio) benzyl)piperidin*-1-yl*)methanone* (**75**). Yellow oil, 51 % yield from **56** and 3-methoxybenzoic acid **73b**. ^{1}H NMR ($CDCl_3$) δ (ppm): 1.10–1.35 (bm, 2H), 1.50–1.90 (bm, 3H), 2.50–2.98 (bm, 4H), 3.67–3.85 (bm, 1H), 3.82 (s, 3H), 4.57–4.80 (bm, 1H), 6.90–6.95 (m, 3H), 7.00–7.03 (m, 1H), 7.18–7.26 (m, 2H), 7.26–7.32 (m, 1H), 7.35–7.43 (m, 2H), 7.46 (dt, 1H, J = 7.8, 1.6 Hz), 8.57 (d, 1H, J = 5.2 Hz).

(3-Methoxyphenyl) (4-(3-((5-(trifluoromethyl)pyridin-2-yl*)thio) benzyl)piperidin*-1-yl*)methanone* (**76**). Yellow oil, 46 % yield from **57** and 3-methoxybenzoic acid **73b**. ^{1}H NMR ($CDCl_3$) δ (ppm): 1.60–1.92 (bm, 5H), 2.60 (d, 2H, J = 8.2 Hz), 2.66–3.01 (bm, 2H), 3.67–3.82 (bm, 1H), 3.82 (s, 3H), 4.50–4.80 (bm, 1H), 6.90–6.96 (m, 4H), 7.23–7.32 (m, 2H), 7.36–7.48 (m, 3H), 7.65 (dd, 1H, J = 8.2, 2.0 Hz), 8.62–8.67 (m, 1H).

(3-Methoxyphenyl) (4-(3-((6-(trifluoromethyl)pyridin-2-yl*)thio) benzyl)piperidin*-1-yl*)methanone* (**77**). Yellow oil, 40 % yield from **58** and 3-methoxybenzoic acid **73b**. ^{1}H NMR ($CDCl_3$) δ (ppm): 1.10–1.35 (bm, 2H), 1.53–1.88 (bm, 3H), 2.60 (d, 2H, J = 6.8 Hz), 2.65–2.97 (bm, 2H), 3.62–3.90 (bm, 1H), 3.81 (s, 3H), 4.50–4.80 (bm, 1H), 6.90–6.95 (m, 3H), 7.01 (d, 1H, J = 8.1 Hz), 7.20–7.25 (m, 1H), 7.26–7.47 (m, 5H), 7.59 (t, 1H, J = 7.9 Hz).

(4-(4-Fluoro-3-((4-(trifluoromethyl)pyridin-2-yl*)thio)benzyl)piperidin*-1-yl*) (3-methoxyphenyl)methanone* (**78**). Yellow oil, 37 % yield from **59** and 3-methoxybenzoic acid **73b**. ^{1}H NMR ($CDCl_3$) δ (ppm): 1.10–1.36 (bm, 2H), 1.53–1.65 (bm, 1H), 1.71–1.86 (bm, 2H), 2.54–2.64 (m, 2H), 2.64–3.00 (bm, 2H), 3.68–3.82 (bm, 1H), 3.82 (s, 3H), 4.62–4.80 (bm, 1H), 6.90–6.96 (m, 3H), 7.01–7.18 (m, 2H), 7.19–7.26 (m, 2H), 7.26–7.33 (m, 1H), 7.36–7.40 (m, 1H), 8.55 (d, 1H, J = 4.2 Hz).

(4-(2-Fluoro-5-((4-(trifluoromethyl)pyridin-2-yl*)thio)benzyl)piperidin*-1-yl*) (3-methoxyphenyl)methanone* (**79**). Yellow oil, 48 % yield from **60** and 3-methoxybenzoic acid **73b.** ^{1}H NMR ($CDCl_3$) δ (ppm): 1.11–1.40 (bm, 2H), 1.55–1.67 (bm, 1H), 1.71–1.92 (bm, 2H), 2.60–2.67 (m, 2H), 2.67–2.80 (bm, 1H), 2.85–3.00 (bm, 1H), 3.68–3.85 (bm, 1H), 3.81 (s, 3H), 4.64–4.73 (bm, 1H), 6.91–6.95 (m, 3H), 7.01–7.04 (m, 1H), 7.13 (t, 1H, J = 8.9 Hz), 7.19 (d, 1H, J = 5.3 Hz), 7.29 (t, 1H, J = 7.8 Hz), 7.40 (dd, 1H, J = 7.1, 2.3 Hz), 7.43–7.48 (m, 1H), 8.55 (d, 1H, J = 5.1 Hz).

(4-(4-Methoxy-3-((4-(trifluoromethyl)pyridin-2-yl*)thio)benzyl)piperidin*-1-yl*) (3-methoxyphenyl)methanone* (**80**). Colorless oil, 44 % yield from **61** and 3-methoxybenzoic acid **73b.** ^{1}H NMR ($CDCl_3$) δ (ppm): 1.10–1.37 (bm, 3H), 1.70–1.84 (bm, 2H), 2.50–2.58 (m, 2H), 2.62–2.80 (bm, 1H), 2.80–3.00 (bm, 1H), 3.69–3.76 (bm, 1H), 3.79 (s, 3H), 3.82 (s, 3H), 4.63–4.77 (bm, 1H), 6.90–6.96 (m, 4H), 6.97–7.00 (m, 1H), 7.14–7.17 (m, 1H), 7.24 (dd, 1H, J = 8.4, 2.3 Hz), 7.28–7.32 (m, 1H), 7.36–7.39 (m, 1H), 8.55 (d, 1H, J = 5.0 Hz).

(4-(2-Methoxy-5-((4-(trifluoromethyl)pyridin-2-yl*)thio)benzyl)piperidin*-1-yl*) (3-methoxyphenyl)methanone* (**81**). Colorless oil, 57 % yield from **62** and 3-methoxybenzoic acid **73b.** ^{1}H NMR ($CDCl_3$) δ (ppm): 1.13–1.39 (bm, 3H), 1.68–1.79 (bm, 1H), 1.79–1.90 (m, 1H), 2.50–2.65 (m, 2H), 2.68–2.78 (bm, 1H), 2.85–2.99 (bm, 1H), 3.68–3.79 (bm, 1H), 3.81 (s, 3H), 3.89 (s, 3H), 4.61–4.74 (bm, 1H), 6.90–6.96 (m, 5H), 7.13–7.16 (m, 1H), 7.28–7.32 (m, 2H), 7.46 (dd, 1H, J = 8.5, 2.4 Hz), 8.55 (d, 1H, J = 5.0 Hz).

(5-Methoxy-2-(phenylthio)phenyl) (4-(3-((4-(trifluoromethyl)pyridin-2-yl*)thio)benzyl)piperidin*-1-yl*)methanone* (**82**). Yellow oil, 27 % yield from **56** and **68a**. ^{1}H NMR ($CDCl_3$) δ (ppm): 0.82–1.17 (bm, 2H), 1.42–1.54 (bm, 1H), 1.66–1.79 (bm, 2H), 2.50–2.91 (bm, 4H), 3.30–3.46 (bm, 1H), 3.82 (s, 3H), 4.65–4.80 (bm, 1H), 6.75–6.90 (m, 2H), 6.97–7.04 (m, 1H), 7.11–7.25 (m, 7H), 7.28–7.48 (m, 4H), 8.57 (d, 1H, J = 5.0 Hz).

(3-Methoxy-5-(phenylthio)phenyl) (4-(3-((4-(trifluoromethyl)pyridin-2-yl*)thio)benzyl)piperidin*-1-yl*)methanone* (**83**). Yellow oil, 28 % yield from **56** and **68b.** ^{1}H NMR ($CDCl_3$) δ (ppm): 0.95–1.12 (bm, 1H), 1.15–1.33 (bm, 1H), 1.47–1.63 (bm, 1H), 1.68–1.84 (bm, 2H), 2.52–2.73 (bm, 3H), 2.78–2.94 (bm, 1H), 3.60–3.73 (bm, 1H), 3.76 (s, 3H), 4.56–4.72 (bm, 1H), 6.76 (dd, 1H, J = 2.4, 1.3 Hz), 6.80 (t, 1H, J = 1.5 Hz), 6.84 (dd, 1H, J = 2.4, 1.6 Hz), 7.00–7.03 (m, 1H), 7.18 (dd, 1H, J = 5.1, 0.9 Hz), 7.21–7.26 (m, 1H), 7.28–7.35 (m, 3H), 7.36–7.43 (m, 4H), 7.46 (dt, 1H, J = 7.8, 1.5 Hz), 8.57 (d, 1H, J = 5. 1 Hz).

(3-Methoxy-4-(phenylthio)phenyl) (4-(3-((4-(trifluoromethyl)pyridin-2-yl*)thio)benzyl)piperidin*-1-yl*)methanone* (**84**). Light yellow solid, 28 % yield from **56** and **68c.** ^{1}H NMR ($CDCl_3$) δ (ppm): 1.10–1.38 (bm, 2H), 1.55–1.68 (bm, 1H), 1.71–1.87 (bm, 2H), 2.55–3.03 (bm, 4H), 3.70–3.87 (bm, 1H), 3.90 (s, 3H), 4.58–4.76 (bm, 1H), 6.81 (d, 1H, J = 8.2 Hz), 6.91 (d, 1H, J = 7.9 Hz), 6.93–6.95 (m, 1H), 6.99–7.02 (m, 1H), 7.18 (d, 1H, J = 4.8 Hz), 7.24 (d, 1H, J = 7.7 Hz), 7.31–7.48 (m, 8H), 7.06 (d, 1H, J = 4.9 Hz).

N-(4-Methoxy-2-(4-(3-((4-(trifluoromethyl)pyridin-2-yl*)thio)benzyl) piperidine-1-carbonyl)phenyl)benzamide* (**85**). Yellow oil, 20 % yield from **56** and **70a**. ^{1}H NMR ($CDCl_3$) δ (ppm): 1.08–1.24 (bm, 2H), 1.60–1.85 (bm, 3H), 2.52 (d, 2H, J = 6.2 Hz), 2.63–3.05 (bm, 2H), 3.81 (s, 3H), 3.82–3.98 (bm, 1H), 4.60–4.76 (bm, 1H), 6.78 (d, 1H, J = 2.9 Hz), 6.98–7.03 (m, 2H), 7.16–7.22 (m, 2H), 7.32–7.35 (m, 1H), 7.38 (t, 1H, J = 7.6 Hz), 7.42–7.56 (m, 4H), 7.88–7.94 (m, 2H), 8.27 (d, 1H, J = 9.0 Hz), 8.56 (d, 1H, J = 5.1 Hz), 9.51 (exchangeable s, 1H).

N-(3-Methoxy-5-(4-(3-((4-(trifluoromethyl)pyridin-2-yl*)thio)benzyl) piperidine-1-carbonyl)phenyl)benzamide* (**86**). Yellow oil, 66 % yield from **56** and **70b**. ^{1}H NMR ($CDCl_3$) δ (ppm): 1.12–1.32 (bm, 2H), 1.57–1.67 (bm, 1H), 1.68–1.85 (bm, 2H), 2.60 (d, 2H, J = 7.1 Hz), 2.63–2.75 (bm, 1H), 2.87–3.02 (bm, 1H), 3.75–3.83 (bm, 1H), 3.83 (s, 3H), 4.57–4.70 (bm, 1H), 6.68 (dd, 1H, J = 2.3, 1.3 Hz), 7.00–7.03 (m, 1H), 7.15 (t, 1H, J = 1.6 Hz), 7.15–7.18 (m, 1H), 7.22–7.25 (m, 1H), 7.36–7.42 (m, 2H), 7.43–7.52 (m, 4H), 7.56 (tt, 1H, J = 7.3, 1.7 Hz), 7.84–7.90 (m, 2H), 8.06 (exchangeable s, 1H), 8.55 (d, 1H, J = 5.1 Hz).

(2-Fluoro-5-methoxyphenyl) (4-(3-((4-(trifluoromethyl)pyridin-2-yl*) thio)benzyl)piperidin*-1-yl*)methanone* (**87**). Yellow oil, 53 % yield from **56** and 2-fluoro-5-methoxybenzoic acid **73a**. ^{1}H NMR ($CDCl_3$) δ (ppm): 1.21–1.37 (bm, 3H), 1.71–1.86 (m, 2H), 2.50–2.65 (m, 2H), 2.65–2.77 (m, 1H), 2.82–3.09 (bm, 1H), 3.50–3.61 (m, 1H), 3.78 (s, 3H), 4.68–4.79 (m, 1H), 6.82–6.90 (m, 2H), 6.97 (t, 1H, J = 8.9 Hz), 7.00–7.03 (m, 1H), 7.15–7.26 (m, 2H), 7.34–7.42 (m, 2H), 7.46 (dt, 1H, J = 7.8, 1.4 Hz), 8.56 (d, 1H, J = 5.1 Hz).

(2-Fluoro-5-methoxyphenyl) (4-(3-((4-(trifluoromethyl)pyridin-2-yl*) thio)benzyl)piperazin*-1-yl*)methanone* (**98**). Light yellow oil, 71 % yield from **97** and 2-fluoro-5-methoxybenzoic acid **73a**. ^{1}H NMR ($CDCl_3$) δ (ppm): 2.37–2.44 (bm, 2H), 2.51–2.57 (m, 2H), 3.30–3.39 (bm, 2H), 3.57 (s, 2H), 3.79 (s, 3H), 3.78–3.83 (bm, 2H), 6.84–6.91 (m, 2H), 6.99 (t, 1H, J = 8.7 Hz), 7.02–7.05 (m, 1H), 7.17–7.20 (m, 1H), 7.40–7.46 (m, 2H), 7.48–7.53 (m, 1H), 7.52–7.60 (m, 1H), 8.57 (d, 1H, J = 5.0 Hz).

4.1.9. General procedure for the synthesis of compounds 12–17, 20–26, 28, 29

A solution of methoxylated amides **74**–**87**, **98** (150 mg, 0.308 mmol) in anhydrous CH_2Cl_2 (3.7 mL) was cooled to −10 °C and treated

dropwise with a 1.0 M solution of BBr_3 in CH_2Cl_2 (1.0 mL) under argon. The mixture was left under stirring at the same temperature for 5 min and then at 0 °C for 1 h and finally at room temperature until starting material was consumed (TLC). The mixture was then diluted with water and extracted with ethyl acetate. The organic phase was washed with brine, dried, and concentrated. The crude product was purified by flash chromatography over silica gel. Elution with CH_2Cl_2 or $CHCl_3$/MeOH (mixtures from 99:1 to 95:5) afforded the desired compounds.

(3-Hydroxyphenyl) (4-(3-((3-(trifluoromethyl)pyridin-2-yl*)thio) benzyl)piperidin*-1-yl*)methanone* (**12**). White solid, 73 % yield from **74**. ^{1}H NMR (DMSO-d_6) δ (ppm): 1.00–1.20 (bm, 2H), 1.43–1.87 (bm, 3H), 2.56 (d, 2H, J = 7.2 Hz), 2.58–2.76 (bm, 1H), 2.82–3.02 (bm, 1H), 3.48–3.64 (bm, 1H), 4.32–4.48 (bm, 1H), 6.67–6.76 (m, 1H), 6.72 (dt, 1H, J = 7.5, 1.3 Hz), 6.80 (ddd, 1H, J = 8.2, 2.5, 1.0 Hz), 7.21 (t, 1H, J = 7.8 Hz), 7.28 (dt, 1H, J = 6.6, 1.8 Hz), 7.31–7.40 (m, 4H), 8.12–8.17 (m, 1H), 8.48–8.52 (m, 1H), 9.65 (exchangeable s, 1H). ^{13}C NMR (DMSO-d_6) δ (ppm): 31.27, 32.02, 37.47, 38.29, 41.62, 47.13, 113.41, 116.23, 117.05, 120.60, 122.20 (q, J = 32.1 Hz), 123.49 (q, J = 272.9 Hz), 128.19, 129.30, 129.58, 130.16, 132.74, 135.49 (q, J = 5.3 Hz), 135.88, 137.75, 141.47, 152.72, 156.70, 157.28, 168.83. HPLC analysis: retention time = 13.149 min; peak area, 98 % (254 nm). HRMS: *m/z* for $C_{25}H_{24}F_3N_2O_2S$ $[M + H]^+$ calculated: 473.15106, found: 473.15018.

(3-Hydroxyphenyl) (4-(3-((4-(trifluoromethyl)pyridin-2-yl*)thio) benzyl)piperidin*-1-yl*)methanone* (**13**). White solid, 69 % yield from **75**. ^{1}H NMR (DMSO-d_6) δ (ppm): 1.02–1.20 (bm, 2H), 1.40–1.70 (bm, 2H), 1.70–1.88 (bm, 1H), 2.59 (d, 2H, J = 7.2 Hz), 2.60–2.73 (bm, 1H), 2.82–3.00 (bm, 1H), 3.50–3.64 (bm, 1H), 4.31–4.48 (bm, 1H), 6.67–6.70 (m, 1H), 6.72 (dt, 1H, J = 7.8, 1.2 Hz), 6.80 (ddd, 1H, J = 8.2, 2.5, 1.0 Hz), 7.06–7.10 (m, 1H), 7.20 (t, 1H, J = 7.8 Hz), 7.32–7.42 (m, 1H), 7.43–7.53 (m, 4H), 8.66 (d, 1H, J = 5.2 Hz), 9.65 (exchangeable s, 1H). ^{13}C NMR (DMSO-d_6) δ (ppm): 31.69, 32.39, 37.94, 41.98, 47.49, 113.83, 115.82 (q, J = 3.9 Hz), 116.10 (q, J = 3.1 Hz), 116.62, 117.41, 122.98 (q, J = 273.7 Hz), 128.79, 129.92, 130.55, 131.26, 133.02, 136.09, 138.00 (q, J = 33.4 Hz), 138.12, 142.87, 151.70, 157.71, 163.32, 169.22. HPLC analysis: retention time = 13.066 min; peak area, 99 % (254 nm). HRMS: *m/z* for $C_{25}H_{24}F_3N_2O_2S$ $[M + H]^+$ calculated: 473.15106, found: 473.15054.

(3-Hydroxyphenyl) (4-(3-((5-(trifluoromethyl)pyridin-2-yl*)thio) benzyl)piperidin*-1-yl*)methanone* (**14**). White solid, 69 % yield from **76**. ^{1}H NMR (DMSO-d_6) δ (ppm): 1.01–1.21 (bm, 2H), 1.44–1.73 (bm, 2H), 1.74–1.90 (bm, 1H), 2.60 (d, 2H, J = 7.8 Hz), 2.64–3.03 (bm, 2H), 3.47–3.70 (bm, 1H), 4.33–4.50 (bm, 1H), 6.66–6.76 (m, 2H), 6.80 (dd, 1H, J = 7.8, 2.1 Hz), 7.04 (d, 1H, J = 8.5 Hz), 7.20 (t, 1H, J = 7.8 Hz), 7.33–7.40 (m, 1H), 7.42–7.52 (m, 3H), 8.01 (dd, 1H, J = 8.5, 2.3 Hz), 8.72–8.80 (m, 1H), 9.65 (exchangeable s, 1H). ^{13}C NMR (DMSO-d_6) δ (ppm): 31.27, 31.89, 37.35, 41.55, 47.08, 113.37, 116.17, 116.98, 120.23, 121.47 (q, J = 32.6 Hz), 123.80 (q, J = 271.9 Hz), 128.12, 129.49, 130.02, 130.87, 132.74, 134.40 (q, J = 3.4 Hz), 135.69, 137.72, 142.38, 146.21 (q, J = 4.2 Hz), 157.25, 166.19, 168.78. HPLC analysis: retention time = 13.184 min; peak area, 98 % (254 nm). HRMS: *m/z* for $C_{25}H_{24}F_3N_2O_2S$ $[M + H]^+$ calculated: 473.15106, found: 473.15012.

(3-Hydroxyphenyl) (4-(3-((6-(trifluoromethyl)pyridin-2-yl*)thio) benzyl)piperidin*-1-yl*)methanone* (**15**). White solid, 63 % yield from **77**. ^{1}H NMR (DMSO-d_6) δ (ppm): 1.02–1.20 (bm, 2H), 1.45–1.90 (bm, 3H), 2.59 (d, 2H, J = 7.2 Hz), 2.62–2.73 (bm, 1H), 2.83–3.00 (bm, 1H), 3.50–3.65 (bm, 1H), 4.30–4.50 (bm, 1H), 6.67–6.70 (m, 1H), 6.72 (dt, 1H, J = 7.6, 1.3 Hz), 6.80 (ddd, 1H, J = 8.2, 2.5, 1.0 Hz), 7.15 (d, 1H, J = 8.1 Hz), 7.20 (t, 1H, J = 7.8 Hz), 7.32–7.39 (m, 1H), 7.42–7.51 (m, 3H), 7.63 (d, 1H, J = 7.2 Hz), 7.91 (t, 1H, J = 7.6 Hz), 9.66 (exchangeable s, 1H). ^{13}C NMR (DMSO-d_6) δ (ppm): 31.35, 32.02, 37.45, 41.66, 47.18, 113.35, 116.19, 117.12, 117.17 (q, J = 3.0 Hz), 121.28 (q, J = 274.1 Hz), 124.29, 128.48, 129.62, 130.04, 130.78, 132.41, 135.52, 137.76, 139.48, 142.37, 146.36 (q, J = 34.1 Hz), 157.15, 162.03, 168.92. HPLC analysis: retention time = 13.238 min; peak area, 98 % (254 nm). HRMS: *m/z* for $C_{25}H_{24}F_3N_2O_2S$ $[M + H]^+$ calculated: 473.15106, found: 473.14984.

(4-(4-Fluoro-3-((4-(trifluoromethyl)pyridin-2-yl*)thio)benzyl)piperidin*-1-yl*) (3-hydroxyphenyl)methanone* (**16**). Beige solid, 71 % yield from **78**. ^{1}H NMR (DMSO-d_6) δ (ppm): 1.01–1.21 (bm, 2H), 1.44–1.70 (bm, 2H), 1.72–1.86 (bm, 1H), 2.57 (d, 2H, J = 6.9 Hz), 2.61–2.75 (bm, 1H), 2.83–3.00 (bm, 1H), 3.50–3.65 (bm, 1H), 4.33–4.50 (bm, 1H), 6.66–6.71 (m, 1H), 6.72 (d, 1H, J = 7.6 Hz), 6.80 (dd, 1H, J = 8.2, 2.2 Hz), 7.20 (t, 1H, J = 7.8 Hz), 7.34 (t, 1H, J = 8.6 Hz), 7.38–7.45 (m, 2H), 7.49–7.56 (m, 2H), 8.63 (d, 1H, J = 5.2 Hz), 9.67 (exchangeable s, 1H). ^{13}C NMR (DMSO-d_6) δ (ppm): 31.19, 31.94, 37.41, 40.67, 41.41, 47.03, 113.37, 115.07 (d, J = 18.5 Hz), 115.80, 116.09, 116.16, 116.38, 116.97, 122.53 (q, J = 273.5 Hz), 129.49 (d, J = 2.3 Hz), 133.35 (d, J = 8.0 Hz), 137.40, 137.62 (q, J = 33.5 Hz), 137.68, 137.80 (d, J = 1.9 Hz), 151.35, 157.25, 160.32, 160.57 (d, J = 245.1 Hz), 168.76. HPLC analysis: retention time = 13.045 min; peak area, 98 % (254 nm). HRMS: *m/z* for $C_{25}H_{23}F_4N_2O_2S$ $[M + H]^+$ calculated: 491.14164, found: 491.14050.

(4-(2-Fluoro-5-((4-(trifluoromethyl)pyridin-2-yl*)thio)benzyl)piperidin*-1-yl*) (3-hydroxyphenyl)methanone* (**17**). Beige solid, 71 % yield from **79**. ^{1}H NMR (DMSO-d_6) δ (ppm): 1.05–1.26 (bm, 2H), 1.43–1.70 (bm, 2H), 1.75–1.90 (bm, 1H), 2.62 (d, 2H, J = 7.0 Hz), 2.63–2.75 (bm, 1H), 2.84–3.03 (bm, 1H), 3.50–3.66 (bm, 1H), 4.32–4.50 (bm, 1H), 6.67–6.72 (m, 1H), 6.72 (d, 1H, J = 7.8 Hz), 6.80 (dd, 1H, J = 8.2, 1.9 Hz), 7.15–7.18 (m, 1H), 7.20 (t, 1H, J = 7.7 Hz), 7.34 (t, 1H, J = 9.0 Hz), 7.49–7.57 (m, 2H), 7.57–7.62 (m, 1H), 8.65 (d, 1H, J = 4.8 Hz), 9.67 (exchangeable s, 1H). ^{13}C NMR (DMSO-d_6) δ (ppm): 31.20, 31.97, 34.76, 36.34, 41.43, 47.01, 113.37, 115.47 (q, J = 3.8 Hz), 115.76, 116.18, 116.97, 117.11 (d, J = 28.4 Hz), 122.55 (q, J = 273.6 Hz), 123.84 (d, J = 3.6 Hz), 128.97 (d, J = 17.4 Hz), 129.49, 135.33, 137.59 (d, J = 33.5 Hz), 137.66, 138.90, 151.27, 157.27, 161.60 (d, J = 245.6 Hz), 162.53, 168.80. HPLC analysis: retention time = 13.149 min; peak area, 97 % (254 nm). HRMS: *m/z* for $C_{25}H_{23}F_4N_2O_2S$ $[M + H]^+$ calculated: 491.14164, found: 491.14059.

(4-(4-Hydroxy-3-((4-(trifluoromethyl)pyridin-2-yl*)thio)benzyl)piperidin*-1-yl*) (3-hydroxyphenyl)methanone* (**20**). White solid, 75 % yield from **80**. ^{1}H NMR (DMSO-d_6) δ (ppm): 1.00–1.17 (bm, 2H), 1.43–1.67 (bm, 2H), 1.67–1.80 (bm, 1H), 2.47 (d, 2H, J = 7.2 Hz), 2.60–2.75 (bm, 1H), 2.82–2.99 (bm, 1H), 3.50–3.64 (bm, 1H), 4.32–4.48 (bm, 1H), 6.67–6.70 (m, 1H), 6.70–6.74 (m, 1H), 6.80 (dd, 1H, J = 8.1, 2.4 Hz), 6.91–6.94 (m, 1H), 6.97 (d, 1H, J = 8.4 Hz), 7.17–7.23 (m, 2H), 7.30 (d, 1H, J = 2.0 Hz), 7.45 (d, 1H, J = 5.2 Hz), 8.64 (d, 1H, J = 5.1 Hz), 9.62 (exchangeable s, 1H). 9.99 (exchangeable s, 1H). ^{13}C NMR (DMSO-d_6) δ (ppm): 31.33, 31.98, 37.62, 40.75, 41.49, 47.04, 113.31, 113.37, 114.54 (q, J = 3.8 Hz), 115.01 (q, J = 3.2 Hz), 116.16, 116.40, 116.97, 122.65 (q, J = 273.5 Hz), 129.47, 131.90, 132.85, 137.10, 137.26 (q, J = 31.8 Hz), 137.72, 150.97, 156.64, 157.24, 163.03, 168.77. HPLC analysis: retention time = 11.826 min; peak area, 96 % (254 nm). HRMS: *m/z* for $C_{25}H_{24}F_3N_2O_3S$ $[M + H]^+$ calculated: 489.14597, found: 489.14502.

(4-(2-Hydroxy-5-((4-(trifluoromethyl)pyridin-2-yl*)thio)benzyl)piperidin*-1-yl*) (3-hydroxyphenyl)methanone* (**21**). White solid, 61 % yield from **81**. ^{1}H NMR (DMSO-d_6) δ (ppm): 1.00–1.20 (bm, 2H), 1.40–1.67 (bm, 2H), 1.79–1.92 (m, 1H), 2.52–2.57 (m, 2H), 2.60–2.74 (bm, 1H), 2.82–3.00 (bm, 1H), 3.50–3.63 (bm, 1H), 4.30–4.45 (bm, 1H), 6.67–6.70 (m, 1H), 6.70–6.73 (m, 1H), 6.80 (ddd, 1H, J = 8.2, 2.4, 0.9 Hz), 6.85–6.88 (m, 1H), 6.93–6.97 (m, 1H), 7.19 (t, 1H, J = 7.9 Hz), 7.29–7.33 (m, 2H), 7.44 (dd, 1H, J = 5.2, 0.9 Hz), 8.65 (d, 1H, J = 5.0 Hz), 9.63 (exchangeable bs, 1H). 10.05 (exchangeable bs, 1H). ^{13}C NMR (DMSO-d_6) δ (ppm): 31.51, 32.24, 35.53, 36.26, 41.48, 47.08, 113.36, 114.22 (q, J = 3.7 Hz), 115.02 (q, J = 3.4 Hz), 116.05, 116.15, 116.81, 116.95, 122.58 (q, J = 273.6 Hz), 128.76, 129.45, 134.91, 137.47 (q, J = 33.3 Hz), 137.72, 138.48, 151.06, 157.25, 157.47, 164.93, 168.80. HPLC analysis: retention time = 11.969 min; peak area, 96 % (254 nm). HRMS: *m/z* for $C_{25}H_{24}F_3N_2O_3S$ $[M + H]^+$ calculated: 489.14597, found: 489.14505.

(5-Hydroxy-2-(phenylthio)phenyl) (4-(3-((4-(trifluoromethyl)pyridin-2-yl*)thio)benzyl)piperidin*-1-yl*)methanone* (**22**). Yellow solid, 74 % yield

from **82**. ^{1}H NMR (DMSO-d_6) δ (ppm): 0.96–1.12 (bm, 1H), 1.34–1.44 (bm, 1H), 1.55–1.80 (bm, 3H), 2.54–2.70 (bm, 3H), 2.77–2.90 (bm, 1H), 3.13–3.25 (bm, 1H), 4.34–4.48 (bm, 1H), 6.60–6.69 (m, 1H), 6.84 (dd, 1H, J = 8.5, 2.1 Hz), 7.00–7.37 (m, 9H), 7.41–7.48 (m, 2H), 7.50 (d, 1H, J = 4.8 Hz), 8.67 (d, 1H, J = 5.1 Hz), 10.15 (exchangeable bs, 1H). ^{13}C NMR (DMSO-d_6) δ (ppm): 31.14, 31.65, 37.26, 40.76, 41.62, 46.39, 113.37, 115.33, 115.68, 116.98, 122.54 (q, J = 273.7 Hz), 125.62, 125.96, 127.10, 128.06, 129.00 (2C), 130.12, 130.81, 132.60, 135.65, 137.55 (q, J = 33.4 Hz), 142.37, 143.27, 143.59, 151.28, 158.37 (2C), 162.94, 166.38, 170.37. HPLC analysis: retention time = 14.533 min; peak area, 98 % (254 nm). HRMS: *m/z* for $C_{31}H_{28}F_3N_2O_2S_2$ $[M + H]^+$ calculated: 581.15443, found: 581.15381.

*(3-Hydroxy-5-(phenylthio)phenyl) (4-(3-((4-(trifluoromethyl)pyridin-*2-yl*)thio)benzyl)piperidin-*1-yl*)methanone* (**23**). White solid, 68 % yield from **83**. ^{1}H NMR (DMSO-d_6) δ (ppm): 0.91–1.14 (bm, 2H), 1.38–1.50 (bm, 1H), 1.52–1.66 (bm, 1H), 1.70–1.86 (bm, 1H), 2.53–2.68 (bm, 3H), 2.78–2.94 (bm, 1H), 3.40–3.56 (bm, 1H), 4.27–4.40 (bm, 1H), 6.55 (t, 1H, J = 1.5 Hz), 6.58 (dd, 1H, J = 2.2, 1.4 Hz), 6.68 (dd, 1H, J = 2.2, 1.8 Hz), 7.07–7.10 (m, 1H), 7.32–7.41 (m, 6H), 7.44–7.52 (m, 4H), 8.67 (d, 1H, J = 5.1 Hz), 9.92 (exchangeable bs, 1H). ^{13}C NMR (DMSO-d_6) δ (ppm): 31.17, 31.84, 37.40, 41.49, 46.99, 56.03, 112.22, 115.41 (q, J = 3.9 Hz), 115.65, 116.66, 117.67, 122.53 (q, J = 273.6 Hz), 128.08, 128.35, 129.70, 130.10, 130.81, 132.00 (2C), 132.58, 133.40, 135.61, 137.16, 137.56 (q, J = 33.4 Hz), 138.53 (2C), 142.38, 151.26, 157.99, 162.85, 167.81. HPLC analysis: retention time = 15.068 min; peak area, 95 % (254 nm). HRMS: *m/z* for $C_{31}H_{28}F_3N_2O_2S_2$ $[M + H]^+$ calculated: 581.15443, found: 581.15332.

*(3-Hydroxy-4-(phenylthio)phenyl) (4-(3-((4-(trifluoromethyl)pyridin-*2-yl*)thio)benzyl)piperidin-*1-yl*)methanone* (**24**). Yellow solid, 61 % yield from **84**. ^{1}H NMR (DMSO-d_6) δ (ppm): 1.03–1.18 (bm, 2H), 1.43–1.70 (bm, 2H), 1.74–1.88 (bm, 1H), 2.59 (d, 2H, J = 6.7 Hz), 2.62–2.73 (bm, 1H), 2.80–3.00 (bm, 1H), 3.52–3.67 (bm, 1H), 4.30–4.45 (bm, 1H), 6.70–6.74 (m, 1H), 6.83–6.87 (m, 1H), 6.96 (d, 1H, J = 7.7 Hz), 7.07–7.10 (m, 1H), 7.26–7.33 (m, 3H), 7.34–7.40 (m, 3H), 7.44–7.52 (m, 4H), 8.67 (d, 1H, J = 4.3 Hz), 10.32 (exchangeable bs, 1H). ^{13}C NMR (DMSO-d_6) δ (ppm): 31.27, 32.03, 37.47, 41.54, 47.11, 113.70, 115.39 (q, J = 3.8 Hz), 115.66, 118.00, 122.26, 122.55 (q, J = 273.6 Hz), 127.25, 128.35, 129.50 (2C), 130.14, 130.80 (3C), 131.11, 132.59, 133.84, 135.66, 136.48, 137.57 (q, J = 33.5 Hz), 142.42, 151.28, 155.49, 162.87, 168.22. HPLC analysis: retention time = 15.090 min; peak area, 98 % (254 nm). HRMS: *m/z* for $C_{31}H_{28}F_3N_2O_2S_2$ $[M + H]^+$ calculated: 581.15443, found: 581.15338.

*N-(4-hydroxy-2-(4-(3-((4-(trifluoromethyl)pyridin-*2-yl*)thio)benzyl) piperidine-1-carbonyl)phenyl)benzamide* (**25**). White solid, 36 % yield from **85**. ^{1}H NMR (DMSO-d_6) δ (ppm): 0.90–1.15 (bm, 2H), 1.35–1.60 (bm, 2H), 1.66–1.79 (bm, 1H), 2.37–2.60 (bm, 3H), 2.81–2.93 (bm, 1H), 3.48–3.62 (bm, 1H), 4.31–4.44 (bm, 1H), 6.66 (d, 1H, J = 1.9 Hz), 6.83 (dd, 1H, J = 8.7, 2.7 Hz), 7.06–7.11 (m, 1H), 7.23–7.37 (m, 3H), 7.40–7.59 (m, 6H), 7.83–7.92 (m, 2H), 8.66 (d, 1H, J = 4.9 Hz), 9.66 (exchangeable bs, 1H), 9.84 (exchangeable s, 1H). ^{13}C NMR (DMSO-d_6) δ (ppm): 31.14, 31.64, 37.18, 41.17, 41.67, 46.81, 113.41, 115.43, 115.71, 116.09, 122.53 (q, J = 273.7 Hz), 126.04, 127.44, 127.93, 128.36 (4C), 130.05, 130.70, 131.45, 132.51, 132.95, 134.43, 135.49, 137.57 (q, J = 33.5 Hz), 142.26, 151.25, 154.81, 162.76, 165.18, 166.99. HPLC analysis: retention time = 13.242 min; peak area, 97 % (254 nm). HRMS: *m/z* for $C_{32}H_{29}F_3N_3O_3S$ $[M + H]^+$ calculated: 592.18817, found: 592.18683.

*N-(3-hydroxy-5-(4-(3-((4-(trifluoromethyl)pyridin-*2-yl*)thio)benzyl) piperidine-1-carbonyl)phenyl)benzamide* (**26**). White solid, 50 % yield from **86**. ^{1}H NMR (DMSO-d_6) δ (ppm): 1.06–1.20 (bm, 2H), 1.48–1.67 (bm, 2H), 1.76–1.87 (bm, 1H), 2.60 (d, 2H, J = 7.2 Hz), 2.64–2.74 (bm, 1H), 2.87–3.00 (bm, 1H), 3.60–3.70 (bm, 1H), 4.34–4.49 (bm, 1H), 6.44 (t, 1H, J = 1.8 Hz), 7.07–7.11 (m, 1H), 7.19–7.22 (m, 1H), 7.36–7.41 (m, 2H), 7.44–7.49 (m, 4H), 7.49–7.55 (m, 2H), 7.59 (tt, 1H, J = 7.4, 2.0 Hz), 7.88–7.96 (m, 2H), 8.65 (d, 1H, J = 5.0 Hz), 9.72 (exchangeable bs, 1H), 10.21 (exchangeable s, 1H). ^{13}C NMR (DMSO-d_6) δ (ppm): 31.21, 32.13, 37.50, 41.58, 47.12, 107.92, 108.82, 109.19, 115.45, 115.67, 122.54 (q, J = 273.4 Hz), 127.68, 128.07, 128.38 (3C), 130.10, 130.81, 131.61, 132.57, 134.92, 135.64, 137.57 (q, J = 33.2 Hz), 137.59, 140.26, 142.41, 151.24, 157.48, 162.83, 165.68, 168.71. HPLC analysis: retention time = 13.265 min; peak area, 96 % (254 nm). HRMS: *m/z* for $C_{32}H_{29}F_3N_3O_3S$ $[M + H]^+$ calculated: 592.18817, found: 592.18683.

*(2-Fluoro-5-hydroxyphenyl) (4-(3-((4-(trifluoromethyl)pyridin-*2-yl*) thio)benzyl)piperidin-*1-yl*)methanone* (**28**). White solid, 38 % yield from **87**. ^{1}H NMR (DMSO-d_6) δ (ppm): 1.00–1.19 (m, 2H), 1.46–1.55 (m, 1H), 1.60–1.69 (m, 1H), 1.74–1.88 (m, 1H), 2.59 (d, 2H, J = 7.2 Hz), 2.64–2.74 (m, 1H), 2.88–3.03 (bm, 1H), 3.34–3.49 (bm, 1H), 4.40–4.48 (m, 1H), 6.59–6.65 (m, 1H), 6.75–6.82 (m, 1H), 7.05 (t, 1H, J = 9.0 Hz), 7.08–7.10 (m, 1H), 7.34–7.39 (m, 1H), 7.43–7.51 (m, 4H), 8.66 (d, 1H, J = 5.2 Hz), 9.61 (exchangeable s, 1H). ^{13}C NMR (DMSO-d_6) δ (ppm): 31.14, 31.92, 37.32, 41.10, 41.42, 46.47, 113.94 (d, J = 3.2 Hz), 115.38 (q, J = 3.8 Hz), 115.62, 116.18, 116.41, 117.08 (d, J = 7.5 Hz), 122.51 (q, J = 273.6 Hz), 124.84 (d, J = 20.3 Hz), 128.38, 130.06, 130.77, 132.52, 135.60, 137.55 (q, J = 33.4 Hz), 142.33, 150.67 (d, J = 235.0 Hz), 151.22, 153.72 (d, J = 1. 8 Hz), 163.25 (d, J = 82.2 Hz). HPLC analysis: retention time = 13.281 min; peak area, 96 % (254 nm). HRMS: *m/z* for $C_{25}H_{23}F_4N_2O_2S$ $[M + H]^+$ calculated: 491.14164, found: 491.14053.

*(2-Fluoro-5-hydroxyphenyl) (4-(3-((4-(trifluoromethyl)pyridin-*2-yl*) thio)benzyl)piperazin-*1-yl*)methanone* (**29**). White solid, 60 % yield from **98**. ^{1}H NMR (DMSO-d_6) δ (ppm): 2.30–2.36 (bm, 2H), 2.38–2.44 (bm, 2H), 3.18–3.24 (bm, 2H), 3.56 (s, 2H), 3.56–3.63 (bm, 2H), 6.34 (dd, 1H, J = 5.4, 3.1 Hz), 6.89 (ddd, 1H, J = 8.9, 4.2, 3.1 Hz), 7.06 (t, 1H, J = 9.0 Hz), 7.15–7.19 (m, 1H), 7.44–7.56 (m, 4H), 7.56–7.58 (m,1H), 8.67 (d, 1H, J = 5.1 Hz), 9.68 (exchangeable s, 1H). ^{13}C NMR (DMSO-d_6) δ (ppm): 41.21, 46.43, 51.98, 52.66, 61.00, 114.10 (d, J = 3.8 Hz), 115.67 (d, J = 3.7 Hz), 115.78, 116.41 (d, J = 24.0 Hz), 117.34 (d, J = 7.7 Hz), 122.53 (q, J = 273.7 Hz), 124.35 (d, J = 19.9 Hz), 128.60, 130.06, 130.63, 133.64, 135.31 (q, J = 8.0 Hz), 137.56 (q, J = 33.4 Hz), 139.97, 150.64 (d, J = 235.3 Hz), 151.30, 153.78, 162.43, 163.79. HPLC analysis: retention time = 12.507 min; peak area, 96 % (254 nm). HRMS: *m/z* for $C_{24}H_{22}F_4N_3O_2S$ $[M + H]^+$ calculated: 492.13689, found: 492.13574.

4.1.10. Synthesis of compounds 18 and 19

To a solution of crude compounds **89** and **90** (300 mg, 1 equiv) in methanol (5.1 mL) was added 1 N aqueous solution of HCl (5.1 mL). The resulting mixture was refluxed until starting material was consumed (2 h). Then the mixture was quenched with H_2O, the organic solvent was removed under reduced pressure. The aqueous phase was extracted with EtOAc, washed with brine and dried over anhydrous Na_2SO_4. The solvent was removed under reduced pressure. Purification by flash chromatography using a mixture of $CHCl_3$/MeOH 98:2 as eluent afforded pure compounds **18** and **19**.

*(3-Hydroxyphenyl) (4-(4-methoxy-3-((4-(trifluoromethyl)pyridin-*2-yl*) thio)benzyl)piperidin-*1-yl*)methanone* (**18**). White solid, 31 % yield from **89**. ^{1}H NMR (DMSO-d_6) δ (ppm): 1.00–1.18 (bm, 2H), 1.41–1.82 (bm, 3H), 2.52–2.55 (m, 2H), 2.60–2.73 (bm, 1H), 2.84–2.99 (bm, 1H), 3.50–3.61 (bm, 1H), 3.72 (s, 3H), 4.34–4.47 (bm, 1H), 6.67–6.70 (m, 1H), 6.72 (d, 1H, J = 7.3 Hz), 6.80 (d, 1H, J = 7.5 Hz), 6.95–6.99 (m, 1H), 7.15 (d, 1H, J = 8.6 Hz), 7.20 (t, 1H, J = 7.9 Hz), 7.33–7.42 (m, 2H), 7.44–7.49 (m, 1H), 8.63 (d, 1H, J = 5.0 Hz), 9.65 (exchangeable bs, 1H). ^{13}C NMR (DMSO-d_6) δ (ppm): 31.27, 31.96, 37.61, 40.67, 41.42, 47.06, 55.92, 112.41, 113.38, 114.78 (q, J = 3.9 Hz), 115.25, 115.50, 116.16, 116.98, 122.61 (q, J = 273.5 Hz), 129.48, 132.84, 133.35, 137.15, 137.48, 137.71, 151.04, 157.26, 157.71, 162.38, 168.76. HPLC analysis: retention time = 12.743 min; peak area, 95 % (254 nm). HRMS: *m/z* for $C_{26}H_{26}F_3N_2O_3S$ $[M + H]^+$ calculated: 503.16162, found: 503.16040.

*(3-Hydroxyphenyl) (4-(2-methoxy-5-((4-(trifluoromethyl)pyridin-*2-yl*) thio)benzyl)piperidin-*1-yl*)methanone* (**19**). White solid, 78 % yield from **90**. ^{1}H NMR (DMSO-d_6) δ (ppm): 1.05–1.20 (bm, 2H), 1.40–1.65 (bm,

2H), 1.76–1.89 (bm, 1H), 2.56 (d, 2H, $J = 7.1$ Hz), 2.84–2.99 (bm, 1H), 3.40–3.48 (m, 1H), 3.50–3.63 (bm, 1H), 3.87 (s, 3H), 4.32–4.45 (bm, 1H), 6.66–6.70 (m, 1H), 6.71 (d, 1H, $J = 7.5$ Hz), 6.80 (dd, 1H, $J = 8.0$, 2.0 Hz), 6.94–6.98 (m, 1H), 7.13 (d, 1H, $J = 8.5$ Hz), 7.19 (t, 1H, $J = 7.9$ Hz), 7.37–7.41 (m, 1H), 7.45–7.48 (m, 1H), 7.49 (dd, 1H, $J = 8.4$, 2.3 Hz), 8.65 (d, 1H, $J = 5.0$ Hz), 9.65 (exchangeable bs, 1H). ^{13}C NMR (DMSO-d_6) δ (ppm): 31.43, 32.20, 35.60, 36.20, 41.40, 47.01, 55.70, 112.46, 113.37, 114.54 (q, $J = 4.0$ Hz), 115.26, 116.15, 116.94, 117.99, 122.57 (q, $J = 273.6$ Hz), 129.46, 130.20, 135.17, 137.50 (q, $J = 33.4$ Hz), 137.69, 137.89, 151.15, 157.27, 158.87, 164.20, 168.77. HPLC analysis: retention time = 13.136 min; peak area, 98 % (254 nm). HRMS: *m/z* for $C_{26}H_{26}F_3N_2O_3S$ $[M + H]^+$ calculated: 503.16162, found: 503.15997.

4.1.11. Procedure for the synthesis of (3-((4-(trifluoromethyl)pyridin-2-yl)thio)phenyl)methanol (94)

To a suspension of lithium aluminium hydride (1.5 equiv) in dry tetrahydrofuran (1.3 mL) at 0 °C, under an argon atmosphere, a solution of compound **93** (200 mg, 1 equiv) in dry tetrahydrofuran (2.6 mL) was added dropwise. The mixture was stirred at room temperature for 1 h, then cooled to 0 °C, quenched with ice and then partitioned between water and ethyl acetate. The organic layer was separated, dried over sodium sulfate, filtered and concentrated. Silica gel column chromatography (eluent: petroleum ether/EtOAc 7:3) afforded the desired compound **94** as a colorless oil (63 % yield). ^{1}H NMR ($CDCl_3$) δ (ppm): 1.81 (exchangeable s, 1H), 4.75 (s, 2H), 7.09–7.12 (m, 1H), 7.18–7.21 (m, 1H), 7.45–7.50 (m, 2H), 7.50–7.55 (m, 1H), 7.61–7.64 (m, 1H), 8.57 (d, 1H, $J = 5.0$ Hz).

4.1.12. Procedure for the synthesis of 2-((3-(bromomethyl)phenyl)thio)-4-(trifluoromethyl)pyridine (95)

Compound **94** (403 mg, 1 equiv) was dissolved in dichloromethane (17.9 mL) under argon atmosphere, cooled to 0 °C, treated dropwise with phosphorus tribromide (0.5 equiv), and stirred for 2 h at room temperature. The mixture was quenched with water, extracted with DCM and the organic phase was washed with brine, dried over sodium sulfate, filtered and concentrated. Silica gel column chromatography (eluent: petroleum ether/EtOAc 95:5) afforded the desired compound **95** as a light yellow oil (40 % yield). ^{1}H NMR ($CDCl_3$) δ (ppm): 4.50 (s, 2H), 7.11–7.14 (m, 1H), 7.19–7.23 (m, 1H), 7.42–7.47 (m, 1H), 7.47–7.51 (m, 1H), 7.51–7.56 (m, 1H), 7.62–7.66 (m, 1H), 8.58 (d, 1H, $J = 5.2$ Hz).

4.1.13. Procedure for the synthesis of compound tert-butyl 4-(3-((4-(trifluoromethyl)pyridin-2-yl)thio)benzyl)piperazine-1-carboxylate (96)

Sodium hydride (60 % dispersion in oil, 1.25 equiv) was added portionwise to a stirred solution of commercially available *tert*-butyl piperazine-1-carboxylate (1 equiv) in dry DMF (3.4 mL) at 0 °C. The mixture was allowed to warm to room temperature over 1 h, then a solution of brominated intermediate **95** (193 mg, 1 equiv) in dry DMF (0.7 mL) was added dropwise and the mixture was stirred at room temperature for 24 h. Water was added and the mixture was extracted with EtOAc. The organic phase was washed with saturated $NaHCO_3$ and brine, dried over sodium sulfate, filtered and concentrated. Silica gel column chromatography (eluent: petroleum ether/EtOAc 7:3) afforded the desired compound **96** as a light-yellow oil (81 % yield). ^{1}H NMR ($CDCl_3$) δ (ppm): 1.45 (s, 9H), 2.34–2.42 (m, 4H), 3.38–3.45 (m, 4H), 3.54 (s, 2H), 7.00–7.04 (m, 1H), 7.16–7.20 (m, 1H), 7.40–7.45 (m, 2H), 7.48–7.53 (m, 1H), 7.56–7.60 (m, 1H), 8.57 (d, 1H, $J = 5.1$ Hz).

4.2. MAGL inhibition assay

Human recombinant MAGL and 4-nitrophenylacetate (4-NPA) were commercially available from Cayman Chemical. IC_{50} values were generated in 96-well microtiter plates. The MAGL reaction was performed at room temperature, at a final volume of 200 μL in 10 mM Tris buffer, pH 7.2, containing 1 mM EDTA and 0.1 mg/mL bovine serum albumin (BSA). A total of 150 μL of 4-NPA 133.3 μM was added to 10 μL of DMSO containing the suitable amount of compound. The reaction was started by adding 40 μL of MAGL (11 ng/well), so that the assay was linear over 30 min. The final concentration of the tested compounds ranged for from 320 to 0.02 nM. After 30 min from the start of the reaction, the absorbance values were measured by using Victor X3 Microplates Reader (PerkinElmer®) at 405 nm. Two reactions were also performed: *1*) a reaction containing no compound and *2*) a reaction containing neither compound nor MAGL. IC_{50} values were derived from experimental data using the Sigmoidal dose−response fitting of GraphPad Prism software. Final values were obtained from duplicates of three independent experiments. To remove possible false-positive results, a blank analysis was performed for each compound concentration, and the final absorbance results were obtained by subtracting the absorbance produced by the presence of all the components except MAGL under the same conditions.

4.3. DTT interference assay

The inhibition assay was the same described above, with the exception that prior to the addition of 40 μL of MAGL (11 ng/well), the compound-substrate mixture was incubated 15 min in the presence of DTT at a 10 μM concentration.

4.4. MAGL preincubation assay

The MAGL reaction was conducted under the same conditions reported above. A total of 150 μL of MAGL (11 ng/well) was added to 10 μL of DMSO containing the appropriate amount of compound. After 0 min, 30 min, and 60 min of incubation time, the reaction was started by adding 40 μL of 4-NPA 500 μM. The enzyme activity was then measured after 30 min from the start of the reaction according to the procedure described above. Final values were obtained from triplicates of two independent experiments.

4.5. MAGL dilution assay

MAGL enzyme (880 ng in 75 μL of Tris buffer, pH 7.2) was incubated for 60 min at room temperature with 5 μL of compound **13**, **16**, **28** and **29** (concentration of 320 nM in the mixture) dissolved in DMSO. The MAGL-inhibitor mixture was then diluted 40-fold with the buffer. After 15 min of incubation, the reaction was started on a 160 μL aliquot by the addition of 40 μL of 4-NPA 500 μM and the enzyme activity was measured according to the procedure described above.

4.6. CB1 and CB2 binding assay

Binding assay to cannabinoid receptor 1 and 2 (CB1 and CB2) were performed as previously described [9]. Briefly, clean membranes expressing *h*CB1 or *h*CB2 were resuspended in binding buffer (50 mM Tris-HCl, 2.5 mM EDTA, 5 mM $MgCl_2$, 0.5 % fatty acid-free BSA, pH 7.4) and incubated with vehicle or compounds and 0.5 nM of [^{3}H]CP55,940 for 90 min at 30 °C. Non-specific binding was determined in the presence of 10 μM of WIN55,512. After incubation, membranes were filtered through a pre-soaked 96-well microplate bonded with GF/B filters under vacuum and washed twelve times with 150 μL of ice-cold binding buffer. The radioactivity was measured and the results expressed as [^{3}H]CP55, 940 binding. Compounds **13, 16, 28** and **29** were tested, at a screening concentration of 10 μM, in two independent experiments, each performed in triplicates.

4.7. Competitive activity-based protein profiling (ABPP)

ABPP experiments were performed using mouse brain membrane preparations at a final concentration of 2 mg/mL in PBS, which were

prepared as described before [23]. Samples (each 19.5 μL of brain membrane homogenates) were preincubated for 25 min at 25 °C with 0.5 μL DMSO (vehicle control) or one of the following inhibitors (final concentration in brackets): compounds **13**, **16**, **28**, **29** (10 μM, MAGL inhibitor), JZL-184 (10 μM, MAGL inhibitor, Cayman Chemical Company), URB597 (4 μM, FAAH inhibitor, Cayman Chemical Company), WWL70 (10 μM, ABHD6 inhibitor, Cayman Chemical Company), THL (30 μM, ABHD6 and 12 inhibitor, Orlistat, Cayman Chemical Company) or MAFP (5 μM, serine hydrolase inhibitor, Abcam Biochemicals). TAMRA-FP (125 nM final concentration) was added to the samples and incubated for 5 min at 25 °C. The reaction was stopped by adding 6.8 μL of 4x Laemmli-buffer with an incubation of 3 min at 25 °C followed by 10 min at 90 °C. The samples were cooled down, centrifuged for 1 min at 10 000 g and separated by electrophoresis in a 10 % SDS-Polyacrylamide Gel (120 V, 180 min). The fluorescent signal in the gel was recorded with a Typhoon FLA 9500 (GE Healthcare Bio-Sciences AB) in TAMRA settings. The presented results were confirmed in two additional independent repetitions of the ABPP experiment.

4.8. Enzyme activity assays

Enzyme activity assays were performed as previously described using intact U937 cells (FAAH and MAGL) and cell homogenates HEK-293 cells stably transfected with ABHD6 and ABHD12 (ABHD6 and ABHD12) [36]. Briefly, MAGL and FAAH activity were determined using U937 cell homogenates (1.0×10^6 cells per sample) which were diluted in 250 μL of Tris-HCl 10 mM, EDTA 1 mM, pH 8, containing 0.1 % fatty acid-free BSA and preincubated with the compounds at different concentrations for 15 min at 37 °C. Then 10 μM of nonradioactive (2-OG) and a small tracer (1 nM) of [^{3}H]2-OG or 100 nM AEA containing 0.5 nM of [ethanolamine-1-^{3}H]AEA were added to the homogenates and incubated for 5 or 15 min, respectively, at 37 °C. The reaction was stopped by the addition of 500 μL of ice-cold $CHCl_3$:MeOH (1:1), and samples were vortexed and rapidly centrifuged at 16000 g for 10 min at 4 °C. The upper aqueous phase was collected in scintillation tubes and mixed with 3 mL of Ultima Gold scintillation liquid (PerkinElmer Life Sciences). The radioactivity associated with [^{3}H]glycerol or [^{3}H]ethanolamine formation for the aqueous phase was measured for tritium content by liquid scintillation spectroscopy. For *h*ABHD6 and *h*ABHD12 activity assays cell homogenates from *h*ABHD6 and *h*ABHD12 stably transfected HEK293 cells were used. Compounds at the screening concentration of 10 μM were pre-incubated with 40 μg of cell homogenate for 30 min at 37 °C and 500 rpm in assay buffer (Tris 1 mM, EDTA 10 mM plus fatty acid-free 0.1 % BSA, pH 7.6). WWL70 10 μM or THL 20 μM were used as positive controls, while DMSO as vehicle control. Then, 10 μM of 2-OG was added and incubated for 5 min at 37 °C. The reaction was stopped by the addition of 400 μL of ice-cold CHCl3:MeOH (1:1) and samples were vortexed and centrifuged (16 000 g, 10 min, 4 °C.). Aliquots (200 μL) of the aqueous phase were assayed for tritium content by liquid scintillation spectroscopy. Blank values were recovered from tubes containing no enzyme, whereas basal 2-OG hydrolysis occurring in non-transfected HEK293 cells was subtracted.

4.9. In vitro ADME assays

4.9.1. UV/LC-MS methods

LC analyses for ADME studies were performed by UV/LC-MS with Agilent 1260 Infinity HPLC-DAD interfaced with an Agilent MSD 6130 (Agilent Technologies, Palo Alto, CA) and an LC−MS/MS system consisting of a Varian apparatus (Varian Inc) including a vacuum solvent degassing unit, two pumps (212-LC), a Triple Quadrupole MSD (Mod. 320-LC) mass spectrometer with ES interface, and Varian MS Workstation System Control Vers. 6.9 software. Chromatographic separation and condition used are the same reported in Bononi et al. [23].

4.9.2. Water solubility

Each solid compound, 1 mg, was added to 1 mL of distilled water. In a shaker water bath, each sample was mixed overnight at room temperature. The resulting suspension was firstly filtered through a 0.45 μm nylon filter and then the solubilized compound was quantified in triplicate using the UV/LC-MS or LC-MS/MS method described above, by comparison with the appropriate calibration curve that was obtained from samples of compounds dissolved in methanol at different concentrations.

4.9.3. Parallel artificial membrane permeability assay (PAMPA)

The PAMPA assay was performed by preparing for each compound a donor solution diluting a stock solution (DMSO, 1 mM) with phosphate buffer (pH 7.4, 25 mM), up to a final concentration of 500 μM. The donor wells were filled with 150 μL of donor solution. The filters were coated with 10 μL of 10 μL of 1 % (w/v) dodecane solution of phosphatidylcholine, instead, the lower wells were filled with 300 μL of acceptor solution (1:1 v/v DMSO and phosphate buffer). The sandwich plate was assembled and incubated for 5 h at room temperature. After the incubation time, plates were separated and the amount of compound in both the donor and acceptor wells was measured by UV/LC-MS. For each compound, the determination was performed in three independent experiments. Permeability (Papp) and Membrane retention percentage (RM%) were calculated according to the equations reported in Bononi et al. [23].

4.9.4. Stability tests

For metabolic stability, DMSO solution of each compound was incubated at 37 °C for 1 h in presence of human liver microsomes (0.2 mg/mL, 5 μL), a NADPH regenerating system (NADPH 0.2 mM, $NADP^+$ 1 mM, D-glucose-6-phosphate 4 mM, 4 unit/mL glucose-6-phosphate dehydrogenase and $MgCl_2$ 48 mM and phosphate buffer (pH 7.4, 25 mM, up to a final volume of 500 μL). The reaction was cooled down in ice and quenched adding acetonitrile (1.0 mL). After centrifugation (4000 rpm for 10 min), the supernatant was taken, dried under nitrogen flow, and suspended in 100 μL of methanol and the parent drug and metabolites were subsequently determined by UV/LC-MS. The percentage of non-metabolized compound was calculated by comparison with reference solutions. For each compound, the determination was performed in three independent experiments. For human plasma stability, instead, each compound (2 mM) was incubated with pooled human plasma (55.7 mg protein/mL), HEPES buffer (25 mM, 140 mM NaCl pH 7.4). The solution was mixed in a test tube that was incubated at 37 °C. At set time points (0.0, 0.25, 0.50, 1.0, 2.0, 4.0, 8.0 and 24.0 h), samples of 100 μL were taken, mixed with 400 μL of cold acetonitrile and centrifuged at 5000 rpm for 15 min. The supernatant was removed and analyzed by UV/LC-MS. For each compound, the determination was performed in three independent experiments.

4.9.5. Animals

Tenebrio molitor coleoptera (TMC) employed in toxicity tests were reared at the University of Siena (Siena, Italy) on a standard diet previously published. Pupae and adult TMC were housed in semi-dark conditions at a temperature of 27 ± 1 °C and a relative humidity level of 40–50 %.

4.9.6. Median lethal dose assessment

TMC were randomly selected and used for analysis within three days after mutation. Compounds **28** and **29** were solubilized in DMSO at the opportune dose expressed in mg/kg of insect weight. One μL of the selected compound has been directly administrated into the hemocoel, between the pronotum and elytron by using a Hamilton syringe, (7001 KH, volume 1 μL, needle size 25 s, cone tip). The range-finding study was conducted with 1 TMC starting from the dose of 200 mg/kg, according to the protocol reported in Brai et al. [35]. The medial lethal dose (LD_{50}) has been determined by injecting the selected dose to five TMC, and

monitoring survival for seven days. The protocol has been repeated until the LD_{50} has been determined using the method reported in Brai et al. [35], and the data confirmed in ten TMC. Data have been analyzed using GraphPad Prism, version 5.04 for Windows (GraphPad Software).

4.10. Docking calculations

The X-ray structure of *h*MAGL (PDB code 5ZUN) [21] energy minimized in explicit water environment, already employed in our previous work [23], was used as receptor for the docking studies of compounds **28** and **29**, which were performed with AUTODOCK 4.0 software [37]. The ligands were built with Maestro [38] and then subjected to energy minimization performed with Macromodel [39] until a convergence value of 0.05 kcal/Å•mol, by employing the CG algorithm, MMFFs force field and a distance-dependent dielectric constant of 1.0. AUTODOCK Tools was used to automatically identify the torsion angles in the ligand, add the solvent model and assign partial atomic charges to the protein and ligands (Kollmann and Gasteiger charges, respectively). The docking site used for calculations was defined in such a way as to contain all residues within a 10 Å shell from the reference ligand in the X-ray crystal structure. The energetic maps were calculated using a grid spacing of 0.375 Å and a distance-dependent function of the dielectric constant. The ligand was subjected to 200 runs of AUTODOCK search using the Lamarckian Genetic Algorithm, following a robust protocol applied in our previous works [40,41]. In particular, for each docking run, 10 000 000 steps of energy evaluations were performed, the number of individuals in the initial population was set to 500 and a maximum of 10 000 000 generations were simulated. An RMS cut-off 2.0 Å was used for pose clustering. All other settings were left as their defaults. The best docked conformation belonging to the best cluster of solutions obtained (top-scored pose) was considered for each ligand.

4.11. MD simulations

MD simulations were performed using Amber20 [42], using the ff14SB force field. General Amber force field (GAFF) parameters were employed for the ligands, whose partial charges were calculated using the Antechamber suite of Amber20, based on the AM1-BCC method. The two analyzed MAGL-ligand complexes produced by docking were placed at the center of a rectangular parallelepiped box and solvated with a 15 Å water cap, generated using TIP3P explicit solvent model. Sodium ions were then added as counterions to neutralize the generated system, which were then energy minimized using a two-step protocol. In the first stage, we kept the protein fixed with a position restraint of 500 kcal/mol·$Å^2$ and we solely minimized the positions of the water molecules. In the second stage, we minimized the entire system through 5000 steps of steepest descent followed by conjugate gradient (CG) until a convergence of 0.05 kcal/Å•mol, applying a position restraint of 10 kcal/mol·$Å^2$ only on the protein α carbons. The minimized complexes were used as input structures for the MD simulations, which were run using Particle Mesh Ewald (PME) electrostatics, a cutoff of 10 Å for the non-bonded interactions and periodic boundary conditions. SHAKE algorithm was used to constrain all bonds involving hydrogen atoms and a time step of 2.0 fs was thus used for the simulation. Initially, a heating stage of 1 ns, in which the temperature of the system was raised from 0 to 300 K, was performed using constant-volume periodic boundary conditions. An equilibration stage of constant-pressure periodic boundary MD was run for 50 ns, keeping the system at the temperature value of 300 K with the Langevin thermostat, for ensuring relaxation of the ligand-protein binding conformation and complex equilibration. Finally, a production step of 1 μs was performed maintaining the same temperature and pressure conditions, and a harmonic potential of 10 kcal/mol•$Å^2$ on the protein α carbons. The final structures of the two different MAGL-ligand complexes corresponded to the average of the last 500 ns of MD simulation minimized by the CG method until a convergence of 0.05 kcal/mol•$Å^2$. The analyses of the MD simulations and the average structures were obtained using the Cpptraj program [43] implemented in Amber20.

Declaration of competing interest

The authors declare that they have no known competing financial interests or personal relationships that could have appeared to influence the work reported in this paper.

Data availability

Data will be made available on request.

Acknowledgments

We are grateful to MIUR (PRIN 2017, project 2017SA5837) and the Italian Ministry of Health – Ricerca Finalizzata 2016 - NET-2016-02363765 for funding. We acknowledge Center for Instrument Sharing of the University of Pisa (CISUP) for the acquisition and elaboration of the high-resolution mass spectra. We thank Livia Pompili for her support to the synthesis of some compounds.

Appendix A. Supplementary data

Supplementary data to this article can be found online at https://doi.org/10.1016/j.ejmech.2023.115916.

References

[1] P. Pacher, S. Bátkai, G. Kunos, The endocannabinoid system as an emerging target of pharmacotherapy, Pharmacol. Rev. 58 (2006) 389–462, https://doi.org/10.1124/pr.58.3.2.
[2] K. Ahn, M.K. McKinney, B.F. Cravatt, Enzymatic pathways that regulate endocannabinoid signaling in the nervous system, Chem. Rev. 108 (2008) 1687–1707, https://doi.org/10.1021/cr0782067.
[3] J.L. Blankman, G.M. Simon, B.F. Cravatt, A comprehensive profile of brain enzymes that hydrolyze the endocannabinoid 2-arachidonoylglycerol, Chem. Biol. 14 (2007) 1347–1356, https://doi.org/10.1016/j.chembiol.2007.11.006.
[4] M.P. Baggelaar, M. Maccarrone, M. van der Stelt, 2-Arachidonoylglycerol: a signaling lipid with manifold actions in the brain, Prog. Lipid Res. 71 (2018) 1–17, https://doi.org/10.1016/j.plipres.2018.05.002.
[5] D.K. Nomura, B.E. Morrison, J.L. Blankman, J.Z. Long, S.G. Kinsey, M.C. G. Marcondes, A.M. Ward, Y.K. Hahn, A.H. Lichtman, B. Conti, B.F. Cravatt, Endocannabinoid hydrolysis generates brain prostaglandins that promote neuroinflammation, Science 334 (2011) 809–813, https://doi.org/10.1126/science.1209200.
[6] F.A. Moreira, M. Grieb, B. Lutz, Central side-effects of therapies based on CB1 cannabinoid receptor agonists and antagonists: focus on anxiety and depression, Best Pract. Res. Clin. Endocrinol. Metabol. 23 (2009) 133–144, https://doi.org/10.1016/j.beem.2008.09.003.
[7] D.K. Nomura, J.Z. Long, S. Niessen, H.S. Hoover, S.W. Ng, B.F. Cravatt, Monoacylglycerol lipase regulates a fatty acid network that promotes cancer pathogenesis, Cell 140 (2010) 49–61, https://doi.org/10.1016/j.cell.2009.11.027.
[8] S. Pisanti, P. Picardi, A. D'Alessandro, C. Laezza, M. Bifulco, The endocannabinoid signaling system in cancer, Trends Pharmacol. Sci. 34 (2013) 273–282, https://doi.org/10.1016/j.tips.2013.03.003.
[9] H. Deng, W. Li, Monoacylglycerol lipase inhibitors: modulators for lipid metabolism in cancer malignancy, neurological and metabolic disorders, Acta Pharm. Sin. B 10 (2020) 582–602, https://doi.org/10.1016/j.apsb.2019.10.006.
[10] J.E. Schlosburg, J.L. Blankman, J.Z. Long, D.K. Nomura, B. Pan, S.G. Kinsey, P. T. Nguyen, D. Ramesh, L. Booker, J.J. Burston, E.A. Thomas, D.E. Selley, L.J. Sim-Selley, Q.S. Liu, A.H. Lichtman, B.F. Cravatt, Chronic monoacylglycerol lipase blockade causes functional antagonism of the endocannabinoid system, Nat. Neurosci. 13 (2010) 1113–1119, https://doi.org/10.1038/nn.2616.
[11] P.K. Chanda, Y. Gao, L. Mark, J. Btesh, B.W. Strassle, P. Lu, M.J. Piesla, M.-Y. Zhang, B. Bingham, A. Uveges, D. Kowal, D. Garbe, E.V. Kouranova, R.H. Ring, B. Bates, M.N. Pangalos, J.D. Kennedy, G.T. Whiteside, T.A. Samad, Monoacylglycerol lipase activity is a critical modulator of the tone and integrity of the endocannabinoid system, Mol. Pharmacol. 78 (2010) 996–1003, https://doi.org/10.1124/mol.110.068304.
[12] U. Taschler, F.P.W. Radner, C. Heier, R. Schreiber, M. Schweiger, G. Schoiswohl, K. Preiss-Landl, D. Jaeger, B. Reiter, H.C. Koefeler, J. Wojciechowski, C. Theussl, J. M. Penninger, A. Lass, G. Haemmerle, R. Zechner, R. Zimmermann, Monoglyceride lipase deficiency in mice impairs lipolysis and attenuates diet-induced insulin resistance, J. Biol. Chem. 286 (2011) 17467–17477, https://doi.org/10.1074/jbc.M110.215434.

[13] S. Ghosh, L.E. Wise, Y. Chen, R. Gujjar, A. Mahadevan, B.F. Cravatt, A.H. Lichtman, The monoacylglycerol lipase inhibitor JZL184 suppresses inflammatory pain in the mouse carrageenan model, Life Sci. 92 (2013) 498–505, https://doi.org/10.1016/j.lfs.2012.06.020.
[14] J.E. Schlosburg, S.G. Kinsey, B. Ignatowska-Jankowska, D. Ramesh, R.A. Abdullah, Q. Tao, L. Booker, J.Z. Long, D.E. Selley, B.F. Cravatt, A.H. Lichtman, Prolonged monoacylglycerol lipase blockade causes equivalent cannabinoid receptor type 1 receptor–mediated adaptations in fatty acid amide hydrolase wild-type and knockout mice, J. Pharmacol. Exp. Therapeut. 350 (2014) 196–204, https://doi.org/10.1124/jpet.114.212753.
[15] J.Z. Long, W. Li, L. Booker, J.J. Burston, S.G. Kinsey, J.E. Schlosburg, F.J. Pavón, A. M. Serrano, D.E. Selley, L.H. Parsons, A.H. Lichtman, B.F. Cravatt, Selective blockade of 2-arachidonoylglycerol hydrolysis produces cannabinoid behavioral effects, Nat. Chem. Biol. 5 (2009) 37–44, https://doi.org/10.1038/nchembio.129.
[16] A.R. King, E.Y. Dotsey, A. Lodola, K.M. Jung, A. Ghomian, Y. Qiu, J. Fu, M. Mor, D. Piomelli, Discovery of potent and reversible monoacylglycerol lipase inhibitors, Chem. Biol. 16 (2009) 1045–1052, https://doi.org/10.1016/j.chembiol.2009.09.012.
[17] A. Chicca, J. Marazzi, J. Gertsch, The antinociceptive triterpene β-amyrin inhibits 2- arachidonoylglycerol (2-AG) hydrolysis without directly targeting cannabinoid receptors, Br. J. Pharmacol. 167 (2012) 1596–1608, https://doi.org/10.1111/j.1476-5381.2012.02059.x.
[18] C. Schalk-Hihi, C. Schubert, R. Alexander, S. Bayoumy, J.C. Clemente, I. Deckman, R.L. DesJarlais, K.C. Dzordzorme, C.M. Flores, B. Grasberger, J.K. Kranz, F. Lewandowski, L. Liu, H. Ma, D. Maguire, M.J. Macielag, M.E. McDonnell, T. M. Haarlander, R. Miller, C. Milligan, C. Reynolds, L.C. Kuo, Crystal structure of a soluble form of human monoglyceride lipase in complex with an inhibitor at 1.35 Å resolution, Protein Sci. 20 (2011) 670–683, https://doi.org/10.1002/pro.596.
[19] G. Hernández-Torres, M. Cipriano, E. Hedén, E. Björklund, A. Canales, D. Zian, A. Feliú, M. Mecha, C. Guaza, C.J. Fowler, S. Ortega-Gutiérrez, M.L. López-Rodríguez, A reversible and selective inhibitor of monoacylglycerol lipase ameliorates multiple sclerosis, Angew. Chem. Int. Ed. 53 (2014) 13765–13770, https://doi.org/10.1002/anie.201407807.
[20] G. Bononi, C. Granchi, M. Lapillo, M. Giannotti, D. Nieri, S. Fortunato, M. El Boustani, I. Caligiuri, G. Poli, K.E. Carlson, S.H. Kim, M. Macchia, A. Martinelli, F. Rizzolio, A. Chicca, J.A. Katzenellenbogen, F. Minutolo, T. Tuccinardi, Discovery of long-chain salicylketoxime derivatives as monoacylglycerol lipase (MAGL) inhibitors, Eur. J. Med. Chem. 157 (2018) 817–836, https://doi.org/10.1016/j.ejmech.2018.08.038.
[21] J. Aida, M. Fushimi, T. Kusumoto, H. Sugiyama, N. Arimura, S. Ikeda, M. Sasaki, S. Sogabe, K. Aoyama, T. Koike, Design, synthesis, and evaluation of piperazinyl pyrrolidin-2-ones as a Novel series of reversible monoacylglycerol lipase inhibitors, J. Med. Chem. 61 (2018) 9205–9217, https://doi.org/10.1021/acs.jmedchem.8b00824.
[22] G. Bononi, G. Tonarini, G. Poli, I. Barravecchia, I. Caligiuri, M. Macchia, F. Rizzolio, G.C. Demontis, F. Minutolo, C. Granchi, T. Tuccinardi, Monoacylglycerol lipase (MAGL) inhibitors based on a diphenylsulfide-benzoylpiperidine scaffold, Eur. J. Med. Chem. 223 (2021), 113679, https://doi.org/10.1016/j.ejmech.2021.113679.
[23] G. Bononi, M. Di Stefano, G. Poli, G. Ortore, P. Meier, F. Masetto, I. Caligiuri, F. Rizzolio, M. Macchia, A. Chicca, A. Avan, E. Giovannetti, C. Vagaggini, A. Brai, E. Dreassi, M. Valoti, F. Minutolo, C. Granchi, J. Gertsch, T. Tuccinardi, Reversible monoacylglycerol lipase inhibitors: discovery of a new class of benzylpiperidine derivatives, J. Med. Chem. 65 (2022) 7118–7140, https://doi.org/10.1021/acs.jmedchem.1c01806.
[24] M.-C. Tung, K.-M. Fung, H.-M. Hsu, T.-S. Tseng, Discovery of 8-prenylnaringenin from hop (Humulus lupulus L.) as a potent monoacylglycerol lipase inhibitor for treatments of neuroinflammation and Alzheimer's disease, RSC Adv. 11 (2021) 31062–31072, https://doi.org/10.1039/D1RA05311F.
[25] J.S. Cisar, O.D. Weber, J.R. Clapper, J.L. Blankman, C.L. Henry, G.M. Simon, J. P. Alexander, T.K. Jones, R.A.B. Ezekowitz, G.P. O'Neill, C.A. Grice, Identification of ABX-1431, a selective inhibitor of monoacylglycerol lipase and clinical candidate for treatment of neurological disorders, J. Med. Chem. 61 (2018) 9062–9084, https://doi.org/10.1021/acs.jmedchem.8b00951.
[26] T. Tuccinardi, C. Granchi, F. Rizzolio, I. Caligiuri, V. Battistello, G. Toffoli, F. Minutolo, M. Macchia, A. Martinelli, Identification and characterization of a new reversible MAGL inhibitor, Bioorg. Med. Chem. 22 (2014) 3285–3291, https://doi.org/10.1016/j.bmc.2014.04.057.
[27] C. Granchi, M. Lapillo, S. Glasmacher, G. Bononi, C. Licari, G. Poli, M. el Boustani, I. Caligiuri, F. Rizzolio, J. Gertsch, M. Macchia, F. Minutolo, T. Tuccinardi, A. Chicca, Optimization of a benzoylpiperidine class identifies a highly potent and selective reversible monoacylglycerol lipase (MAGL) inhibitor, J. Med. Chem. 62 (2019) 1932–1958, https://doi.org/10.1021/acs.jmedchem.8b01483.
[28] M.J. Niphakis, B.F. Cravatt, Enzyme inhibitor discovery by activity-based protein profiling, Annu. Rev. Biochem. 83 (2014) 341–377, https://doi.org/10.1146/annurev-biochem-060713-035708.
[29] J.L. Blankman, B.F. Cravatt, Chemical probes of endocannabinoid metabolism, Pharmacol. Rev. 65 (2013) 849–871, https://doi.org/10.1124/pr.112.006387.
[30] D. Piomelli, G. Tarzia, A. Duranti, A. Tontini, M. Mor, T.R. Compton, O. Dasse, E. P. Monaghan, J.A. Parrott, D. Putman, Pharmacological profile of the selective FAAH inhibitor KDS-4103 (URB597), CNS Drug Rev. 12 (2006) 21–38, https://doi.org/10.1111/j.1527-3458.2006.00021.x.
[31] W. Li, J.L. Blankman, B.F. Cravatt, A functional proteomic strategy to discover inhibitors for uncharacterized hydrolases, J. Am. Chem. Soc. 129 (2007) 9594–9595, https://doi.org/10.1021/ja073650c.
[32] H.S. Hoover, J.L. Blankman, S. Niessen, B.F. Cravatt, Selectivity of inhibitors of endocannabinoid biosynthesis evaluated by activity-based protein profiling, Bioorg. Med. Chem. Lett. 18 (2008) 5838–5841, https://doi.org/10.1016/j.bmcl.2008.06.091.
[33] D.G. Deutsch, R. Omeir, G. Arreaza, D. Salehani, G.D. Prestwich, Z. Huang, A. Howlett, Methyl arachidonyl fluorophosphonate: a potent irreversible inhibitor of anandamide amidase, Biochem. Pharmacol. 53 (1997) 255–260, https://doi.org/10.1016/S0006-2952(96)00830-1.
[34] M.P. Baggelaar, F.J. Janssen, A.C.M. van Esbroeck, H. den Dulk, M. Allarà, S. Hoogendoorn, R. McGuire, B.I. Florea, N. Meeuwenoord, H. van den Elst, G. A. van der Marel, J. Brouwer, V. Di Marzo, H.S. Overkleeft, M. van der Stelt, Development of an activity-based probe and in silico design reveal highly selective inhibitors for diacylglycerol lipase-α in brain, Angew. Chem. Int. Ed. 52 (2013) 12081–12085, https://doi.org/10.1002/anie.201306295.
[35] A. Brai, F. Poggialini, C. Vagaggini, C. Pasqualini, S. Simoni, V. Francardi, E. Dreassi, Tenebrio molitor as a simple and cheap preclinical pharmacokinetic and toxicity model, Int. J. Mol. Sci. 24 (2023) 2296, https://doi.org/10.3390/ijms24032296.
[36] C. Granchi, G. Bononi, R. Ferrisi, E. Gori, G. Mantini, S. Glasmacher, G. Poli, S. Palazzolo, I. Caligiuri, F. Rizzolio, V. Canzonieri, T. Perin, J. Gertsch, A. Sodi, E. Giovannetti, M. Macchia, F. Minutolo, T. Tuccinardi, A. Chicca, Design, synthesis and biological evaluation of second-generation benzoylpiperidine derivatives as reversible monoacylglycerol lipase (MAGL) inhibitors, Eur. J. Med. Chem. 209 (2021), 112857, https://doi.org/10.1016/j.ejmech.2020.112857.
[37] G.M. Morris, R. Huey, W. Lindstrom, M.F. Sanner, R.K. Belew, D.S. Goodsell, A. J. Olson, AutoDock4 and AutoDockTools4: automated docking with selective receptor flexibility, J. Comput. Chem. 30 (2009) 2785–2791, https://doi.org/10.1002/jcc.21256.
[38] Schrödinger Maestro, Inc., New York, 2016 version 10.6.
[39] Schrödinger Macromodel, Inc., New York, 2009 version 9.7.
[40] A. Bisio, M. De Mieri, L. Milella, A.M. Schito, A. Parricchi, D. Russo, S. Alfei, M. Lapillo, T. Tuccinardi, M. Hamburger, N. De Tommasi, Antibacterial and hypoglycemic diterpenoids from salvia chamaedryoides, J. Nat. Prod. 80 (2017) 503–514, https://doi.org/10.1021/acs.jnatprod.6b01053.
[41] G. Poli, A. Gelain, F. Porta, A. Asai, A. Martinelli, T. Tuccinardi, Identification of a new STAT3 dimerization inhibitor through a pharmacophore-based virtual screening approach, J. Enzym. Inhib. Med. Chem. 31 (2016) 1011–1017, https://doi.org/10.3109/14756366.2015.1079184.
[42] D.A. Case, T.E. Cheatham, T. Darden, H. Gohlke, R. Luo, K.M. Merz, A. Onufriev, C. Simmerling, B. Wang, R.J. Woods, The Amber biomolecular simulation programs, J. Comput. Chem. 26 (2005) 1668–1688, https://doi.org/10.1002/jcc.20290.
[43] D.R. Roe, T.E. Cheatham, PTRAJ and CPPTRAJ: software for processing and analysis of molecular dynamics trajectory data, J. Chem. Theor. Comput. 9 (2013) 3084–3095, https://doi.org/10.1021/ct400341p.